POLITECNICO DI TORINO

Master's Degree in Mechatronic Engineering - Control Technologies for Industry 4.0

Master's Degree Thesis

A Pontryagin-based NMPC approach for a LEO to GEO transfer space mission

Supervisors

Prof. Carlo NOVARA

Prof. Michele PAGONE

Candidate

Salvatore DI FATTA

24th October 2022

I

Acknowledgements

To my family

Table of Contents

Acronyms

AOCS

Attitude and Orbit Control System

CoM

Center of Mass

ECI

Earth-Centered Inertial Frame

ESA

European Space Agency

FR2B

Free Restricted Two-Body Equation

GE

Geocentric Equatorial Frame

GEO

Geostationary Orbit

KEO

Keplerian Orbital Elements

LEO

Low Earth Orbit

LORF

Local Orbit Frame

LVLH

Local Vertical Local Horizontal Frame

MEOE

Modified Equinoctial Orbital Element

MPC

Model Predictive Control

NMPC

Nonlinear Model Predictive Control

ORE

Orbit Equation

PF

Perifocal (Perigee) Frame

PMP

Pontryagin Minimum (or Maximum) Principle

RIC

Radial In-track Cross-track Frame

R2B

Restricted Two-Body Equation

S/C

Spacecraft

SROC

Space Rider Observer Cube

List of Figures

List of Tables

Chapter 1

Introduction

As explained in [1], a satellite or artificial satellite is an object intentionally placed into orbit in outer space in order to perform a specific task. Since the launch cost is really expensive, satellites are designed to be as lightweight and robust as possible. They are placed from the surface to orbit by launcher, high enough to avoid orbital decay by the atmosphere. They can move to or maintain the orbit by propulsion, usually by chemical or ion thrusters. Almost all the satellites orbiting Earth are in low Earth orbit (LEO) or geostationary orbit (GEO); let's focus on the main characteristic of these two orbits.

1.1   Low Earth Orbit - LEO

As reported in [2], A low Earth orbit (LEO) is defined as an orbit around Earth with a period of 2 hours and 8 minutes or less (at least 11.25 orbits per day) and an eccentricity of less than 0.25. The majority of man-made objects in space are in LEO, with an altitude of no more than one-third the radius of Earth.
The word LEO region also refers to the area of space below 2,000 km (about a third of Earth's radius). Objects in orbit that pass through this zone are strictly monitored, even if their apogee is further out or they are sub-orbital, since they represent a potential collision to the many LEO satellites.

1.1.1   Applications

A low Earth orbit requires a very low amount of energy in order to place a satellite. It provides high bandwidth and low communication latency. Satellites and space stations in LEO are more accessible for crew and servicing.
Since it requires less energy to place a satellite into a LEO, and a satellite there needs less powerful amplifiers for successful transmission, LEO is used for many

communication applications, such as the Iridium phone system. Some communication satellites use much higher geostationary orbits and move at the same angular velocity as the Earth as to appear stationary above one location on the planet.

1.1.2 Advantages

As explained in [3], the following are the benefits of LEO orbit:

- Because they are close to the earth, LEO satellites launched in LEO orbit give stronger signal strength. As a result, less power (approximately 1 W) is required for transmission.

- Because of its proximity to the Earth, it has the shortest propagation delay (approximately 10ms) when compared to other orbits. It can be utilised for real-time time sensitive applications because of its low latency.

- Low-cost satellite equipment is enough for ground stations.

- Smaller footprints allow for better frequency reuse.

- It offers great elevation for the Earth's polar regions. As a result, more worldwide coverage is possible.

1.1.3 Disadvantages

The following are the primary drawbacks:

- Because it is at a lower altitude above the Earth, it covers a smaller area. As a result, a vast number of satellites are required to cover the whole Earth's surface (see Starlink constellation by SpaceX). However, the installation of such LEO-based systems is costly.

- Because LEO satellites move continually, service is passed from one satellite to the next in the constellation. As a result, a series of satellites is necessary to cover any part of the Earth.

- Atmospheric influences are greater, causing progressive orbital disorientation of satellites. This necessitates regular satellite maintenance to maintain them in LEO orbit.

- It is only visible for 15 to 20 minutes from a certain location on Earth. As a result, there is less time in order to test and debug.

- The efficiency of serving inhabited areas is lower than that of GEO satellites.

- Ground stations are quite complicated because they must handle frequent hand-offs between LEO satellites.

- LEO satellites have a shorter life period (5 to 8 years) than GEO ones (about a decade).

1.1.4   Examples

Referring to [2], The following are the most important examples of LEO satellites and space stations:

- The International Space Station (ISS) is in a low-Earth orbit (LEO) 400 to 420 kilometres above the Earth's surface and requires re-boost a few times a year owing to orbital degradation.

- The Iridium communications satellites orbit at a height of around 780 kilometres.

- Earth observation spacecraft, also known as remote sensing satellites, such as spy satellites and other Earth imaging satellites, employ LEO because they can view the Earth's surface more clearly because they are closer to it.

- The Hubble Space Telescope orbits around the Earth at 540 kilometres of altitude.

- The Chinese Tiangong space station is now orbiting between 340 and 450 kilometres above the Earth.

1.2   Geostationary Orbit - GEO

As reported in [4], A Geostationary Orbit (GEO), usually known as a Geosynchronous Equatorial Orbit (GEO), is a circular geosynchronous orbit 35,786 kilometers above Earth's Equator (42,164 km radius from Earth's centre) that follows the rotation of the Earth.
An object in such an orbit has an orbital period equal to Earth's rotational cycle, one sidereal day, and hence appears immobile in the sky to ground observers.

1.2.1   Applications

1. **Communication**: Geostationary communication satellites are utilised because they can be seen from a wide portion of the Earth's surface, spanning 81 degrees in both latitude and longitude. They have crossed the equator. It looks lower in the sky to observers near the pole. It eliminates the requirement

for ground stations on Earth to have mobile antennas, allowing an observer to employ small, inexpensive, fixed antennas that are aimed towards the target satellites.

2. **Meteorology**: These satellites are utilised in meteorology as well. Infrared photographs of the Earth's surface and atmosphere are provided by geostationary meteorological satellites. They are employed in oceanography as well as atmospheric tracking.
   They take photos in the visible and infrared spectrums and assist us in tracking numerous weather phenomena such as volcanic ash, cloud temperatures, oceanography, temperature and vegetation covering, cyclonic course, and so on.

3. **Navigation**: For navigation, a system known as the Global Navigation Satellite System (GNSS) is employed. Relaying clocks, ephemeris, and ionospheric error corrections employ this. They serve as an extra reference signal.

1.2.2   Advantages

Below the main advantages, as reported in [5]:

- Because it is higher up, it covers a bigger geographical region. As a result, only three satellites are necessary to cover the whole Earth.

- Satellites may be seen for 24 hours straight from a single fixed place on Earth.

- It is perfect for broadcasting and multi-point distribution.

- Ground station tracking is unnecessary since the fixed position is always visible from Earth.

- No inter-satellite handoff is required.

- Fewer satellites are required to cover the whole globe. Three satellites are more than enough for the purpose.

- Because there is almost no doppler shift, fewer complicated receivers may be employed for satellite communication.

1.2.3 Disadvantages

Below the main disadvantages:

- The signal takes a long time to get from Earth to satellite and vice versa. In one direction, the signal travel delay is roughly 120ms. With a signal speed of 3x108 m/sec and a distance of 35786 Km, the delay is 120 ms. As a result, it is unsuitable for point-to-point applications that need time-critical applications such as real-time speech, video, and so on.

- From the moment that GEO orbit is positioned above the equator, broadcasting near the poles is problematic.

- The received signal is quite weak due to the extended transmission distance. Better LNA (Low Noise Amplifier) and sophisticated signal processing techniques in the satellite modem are required. This raises the cost of ground station equipment.

- It has low coverage at higher latitudes, often greater than 77 degrees.

1.2.4 Examples

Meteorology

- NOAA's GOES series performed by the United States

- the Meteosat satellite series, which was launched by the European Space Agency and is administered by the European Weather Satellite Organization, EUMETSAT.

- COMS-1 and GK-2A multi-mission satellites from the Republic of Korea

- the Russian Elektro-L satellite constellation

- the Himawari series from Japan

- Chinese Fengyun series

- India's INSAT satellite series

Navigation

- The WAAS, i.e. the Wide Area Augmentation System, provided by the United States Federal Aviation Administration.

- The EGNOS, that is The European Geostationary Navigation Overlay Service, managed by the ESSP.

- The Multi-functional Satellite Augmentation System (MSAS), administered by Japanese Government.

- India's GPS Aided Geo Augmented Navigation (GAGAN) system.

- The commercial StarFire navigation system.

- Fugro's commercial Starfix DGPS System and OmniSTAR system.

1.3   Objectives and outline of the thesis

Nowadays, the propellant consumption minimization is a fundamental task for space missions in order to save more money budget and to plan a longer duration for them. As stated in [6], in the last years space technology has moved forward, overcoming classical astrodynamics methods as the Lambert's problem solution and the Hohmann transfer which are ideal and open-loop maneuvers that require a strong human effort.
As it has been seen in control system literature, a MPC-based control strategy is a very interesting solution because allows us to deal with linear and nonlinear systems, to impose input and/or state constraints, to have a guidance and control strategy managed by a single algorithm and most important to have an optimum trade-off between performances and fuel consumption.

The work of thesis consists into design a control algorithm through a Nonlinear Model Predictive Control approach in order to transfer a spacecraft from a Low Earth Orbit (LEO) to a Geostationary Orbit (GEO). Instead of using the classical numerical optimization approach, an analytical method based on Pontryagin Minimum (or Maximum) Principle has been involved [7], allowing to get an explicit optimal control law. Both the dynamical and internal prediction models, used for designing and simulating purposes, are based on the Modified Equinoctial Orbital Elements, a set of six equations that allows us to overcome some singularities that would be present using the standard Keplerian elements.

The thesis is organized in six chapters, including the current Chapter 1, that introduces some notions about LEO and GEO orbits and highlights the aim of the thesis.

Chapter 2 deals with the S/C dynamics and so the orbital elements required to define the control problem.

Chapter 3 provides an overview of the Nonlinear Model Predictive Control (NMPC) technique utilised to complete the mission.

Chapter 4 describes the mission scenario.

Chapter 5 presents the results obtained by applying the Pontryagin-based NMPC approach.

Chapter 6 summarises some last thoughts on the thesis work and suggests possible future advances.

Chapter 2

Orbital Mechanics

Spacecrafts are complex vehicles designed to fly in outer space. They are mainly employed for communications, Earth observation, meteorology, navigation, space colonization, planetary exploration, and transportation of humans and cargo. As expressed more specifically in [8], a spacecraft can be seen as a rigid body which moves with respect to some Inertial frame of reference. Its motion is a roto-translational one, i.e. composed of a translation of the body Center of Mass (CoM) plus a rotation of the body about an axis passing through the CoM. As regards the translational motion, reference can be made to the theory of Orbital Mechanics and Celestial Mechanics, which depends on the ideas born of brilliant minds such as those of the scientists Newton and Kepler.

2.1 Newton's laws

The contribution and the studies made by Isaac Newton have been fundamental not only for aerospace applications but in general for all science. In particular, he presented the principles (three laws of motion and one law of gravitation) all together in 1687 in the work Philosophiae Naturalis Principia Mathematica (The mathematical principles of natural philosophy), which will be reported below:

1. Unless acted upon by an external force, a particle remains at rest or moves at a fixed velocity.

2. The rate of change of the linear momentum $m\mathbf{v}$ of a particle is given by

$$\frac{d}{dt}(m\mathbf{v}) = \mathbf{F} \tag{2.1}$$

   where m is the particle mass, $\mathbf{v}$ the particle velocity and $\mathbf{F}$ the force acting on the particle.

3. There exists a force $\mathbf{F}_{21} = -\mathbf{F}_{12}$ exerted by particle 2 on particle 1 for every force $\mathbf{F}_{12}$ exerted by particle 1 on particle 2.

4. Any two particles attract each other with a force

$$\mathbf{F} = \frac{Gm_1m_2\mathbf{r}}{r^3} \tag{2.2}$$

where m_1, m_2 are the particle masses, $\mathbf{r}$ vector of magnitude r, r the distance connecting the two particles and $G = 6.67 \times 10^{-11} \, \mathrm{Nm^2/kg^2}$ the universal constant of gravitation.

2.2 Kepler's laws

From these more general laws, Kepler's laws of planetary motion can be derived as consequence, obtaining the following results:

1. A planet's orbit is an ellipse with the sun at one focus.

2. The radius vector traced from the sun to a planet sweeps out equal areas at equal intervals of time (i.e. the areal velocity is constant).

3. Planetary periods of revolution are proportional to $r_m^{3/2}$, where r_m is the mean distance from the sun.

2.3 Two-body problem

Given this general setting, the goal is to derive a mathematical model able to describe the dynamics of a body orbiting around an other body, for example a S/C orbiting around a planet. Let's consider the following scenario:
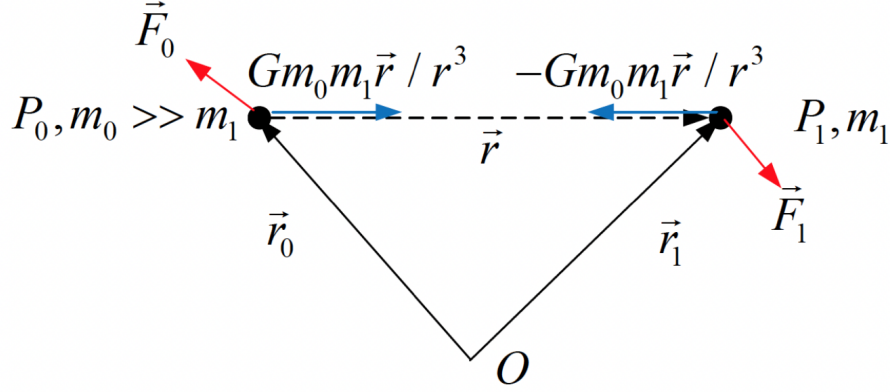
Figure 2.1: General setting Two-body problem from [8]

where m_0 and m_1 are the two particle masses, located respectively at positions P_0 and P_1 in an inertial frame with origin in O, $\mathbf{r}_0$ and $\mathbf{r}_1$ the position vectors of the masses, $\mathbf{r} = \mathbf{r}_1 - \mathbf{r}_0$ the relative position, $\mathbf{v}_0$ and $\mathbf{v}_1$ the velocities of the masses, $\mathbf{F}_0$ and $\mathbf{F}_1$ the external forces (non gravitational) acting on the masses.

Assuming that masses are constant, using jointly (2.1) and (2.2), we are able to write down the following equations:

$$\dot{\mathbf{v}}_0 = \frac{Gm_1}{r^3}\mathbf{r} + \frac{1}{m_0}\mathbf{F}_0 \tag{2.3}$$

$$\dot{\mathbf{v}}_1 = -\frac{Gm_0}{r^3}\mathbf{r} + \frac{1}{m_1}\mathbf{F}_1 \tag{2.4}$$

making some transformations, we can put in evidence the relative motion of the two masses and their CoM motion. In particular:

$$\mathbf{r} = \mathbf{r}_1 - \mathbf{r}_0 \qquad \text{(Relative position)}$$

$$\mathbf{v} = \mathbf{v}_1 - \mathbf{v}_0 \qquad \text{(Relative velocity)}$$

$$\mathbf{r}_c = \frac{m_0}{m_0 + m_1}\mathbf{r}_0 + \frac{m_1}{m_0 + m_1}\mathbf{r}_1 \qquad \text{(CoM position)}$$

$$\mathbf{v}_c = \frac{m_0}{m_0 + m_1}\mathbf{v}_0 + \frac{m_1}{m_0 + m_1}\mathbf{v}_1 \qquad \text{(CoM velocity)}$$

from the above equations we obtain:

$$\dot{\mathbf{v}} = -\frac{G\left(m_0 + m_1\right)}{r^3}\mathbf{r} + \frac{1}{m_1}\left(\mathbf{F}_1 - \frac{m_1}{m_0}\mathbf{F}_0\right) \tag{2.5}$$

$$\dot{\mathbf{v}}_c = \frac{\mathbf{F}_0 + \mathbf{F}_1}{m_0 + m_1} \tag{2.6}$$

where (2.5) and (2.6) represent respectively the relative motion and the CoM motion. As can be noticed, for $m_0 \gg m_1$ the acceleration of CoM $\dot{\mathbf{v}}_c = 0 \rightarrow \mathbf{v}_c = \text{const}$, in other words, the CoM can be selected as the origin of an inertial frame of reference. Instead, the (2.5) get the following form, better known as *Restricted Two-body equation*:

$$\dot{\mathbf{v}} + \mu \frac{\mathbf{r}}{r^3} = \frac{1}{m_1}\mathbf{F}_1 \tag{R2B}$$

where $\mu = Gm_0$ is the gravitational parameter.

2.4 Free restricted Two-body problem

Considering the homogeneous differential equation version of (R2B), that is:

$$\dot{\mathbf{v}} + \mu \frac{\mathbf{r}}{r^3} = 0 \tag{FR2B}$$

we are able to derive some important mechanical and geometrical results, as explained in [8]. Will be analyzed:

1. The total mechanical energy of the FR2B system is conserved;

2. The angular momentum of the FR2B system is conserved;

3. The free response of the FR2B equation occurs on a plane;

4. Geometric description of the FR2B trajectories (orbits).

2.4.1 Energy conservation

Take the dot product of equation (FR2B) with $\mathbf{v}$:

$$\begin{aligned}
\dot{\mathbf{v}} \cdot \mathbf{v} + \frac{\mu}{r^3}\mathbf{r} \cdot \mathbf{v} &= \frac{1}{2}\frac{d}{dt}(\mathbf{v} \cdot \mathbf{v}) + \frac{\mu}{2r^3}\frac{d}{dt}(\mathbf{r} \cdot \mathbf{r}) \\
&= \frac{d}{dt}\frac{v^2}{2} + \frac{\mu}{2r^3}\frac{d}{dt}r^2 = \frac{d}{dt}\frac{v^2}{2} + \frac{\mu\dot{r}}{r^2} = \frac{d}{dt}\left(\frac{v^2}{2} - \frac{\mu}{r}\right) = 0
\end{aligned} \tag{2.7}$$

This demonstrates the energy conservation principle:

$$\dot{\mathcal{E}} = 0, \quad \mathcal{E} = \text{const} \tag{2.8}$$

where:

* $\mathcal{E} = \frac{v^2}{2} - \frac{\mu}{r}$ is the total mechanical energy per unit mass

11

* $\frac{v^2}{2}$ is the kinetic energy per unit mass

* $-\frac{\mu}{r}$ is the potential energy per unit mass

Moreover, given a constant total mechanical energy $\mathcal{E}$, the resulting orbital velocity is $v = \sqrt{2\mu/r + 2\mathcal{E}}$.

2.4.2 Angular momentum conservation and planar motion

Consider the cross product between $\mathbf{r}$ and equation (FR2B):

$$\mathbf{r} \times \dot{\mathbf{v}} + \frac{\mu}{r^3}\mathbf{r} \times \mathbf{r} = \mathbf{r} \times \dot{\mathbf{v}} = \mathbf{v} \times \mathbf{v} + \mathbf{r} \times \dot{\mathbf{v}} = \frac{d}{dt}(\mathbf{r} \times \mathbf{v}) = \mathbf{0} \qquad (2.9)$$

This demonstrates the angular momentum conservation principle:

$$\dot{\mathbf{h}} = \mathbf{0}, \quad \mathbf{h} = \text{ const} \qquad (2.10)$$

where:

* $\mathbf{h} = \mathbf{r} \times \mathbf{v}$ is the angular momentum per unit mass

The fact that $\mathbf{h}$ is constant implies that $\mathbf{r}$ and $\mathbf{v}$ are coplanar. The plane in which they are located is known as the *orbital plane*.

2.4.3 Orbit equation

Take the cross product of equation (FR2B) with $\mathbf{h}$:

$$\left(\dot{\mathbf{v}} + \frac{\mu}{r^3}\mathbf{r}\right) \times \mathbf{h} = \frac{d}{dt}\left(\mathbf{v} \times \mathbf{h} - \frac{\mu}{r}\mathbf{r}\right) = 0 \qquad (2.11)$$

the preceding equation demonstrates that:

$$\mathbf{v} \times \mathbf{h} - \frac{\mu}{r}\mathbf{r} = \text{const} = \mu\mathbf{e} \qquad (2.12)$$

where $\mathbf{e}$ is the *eccentricity vector* and $e = |\mathbf{e}|$ is the *eccentricity*.

Take the dot product between $\mathbf{r}$ and equation (2.12):

$$\mathbf{r} \cdot (\mathbf{v} \times \mathbf{h}) - \frac{\mu}{r}\mathbf{r} \cdot \mathbf{r} = \mu\mathbf{r} \cdot \mathbf{e} \qquad (2.13)$$

knowing that $\mathbf{r} \cdot (\mathbf{v} \times \mathbf{h}) = (\mathbf{r} \times \mathbf{v}) \cdot \mathbf{h}$ (Scalar triple product) and $(\mathbf{r} \times \mathbf{v}) \cdot \mathbf{h} = \mathbf{h} \cdot \mathbf{h} = h^2$ we obtain:

$$h^2 - \mu r = \mu r e \cos\theta \qquad (2.14)$$

12

where θ (the angle between **r** and **e**) is known as *true anomaly.*

We get the *orbit equation* by explicitly setting $p = h^2/\mu$ (where p is known as the *parameter* or *semilatus rectum*) and expressing the above equation with respect to r. The equation obtained is the following:

$$r = \frac{p}{1 + e\cos\theta} \tag{ORE}$$

2.5   Orbit geometry

The (ORE) is the equation of a *conic section*, written in polar terms r and θ (where $\theta \in [0, 2\pi]$). Below all the possible configurations:
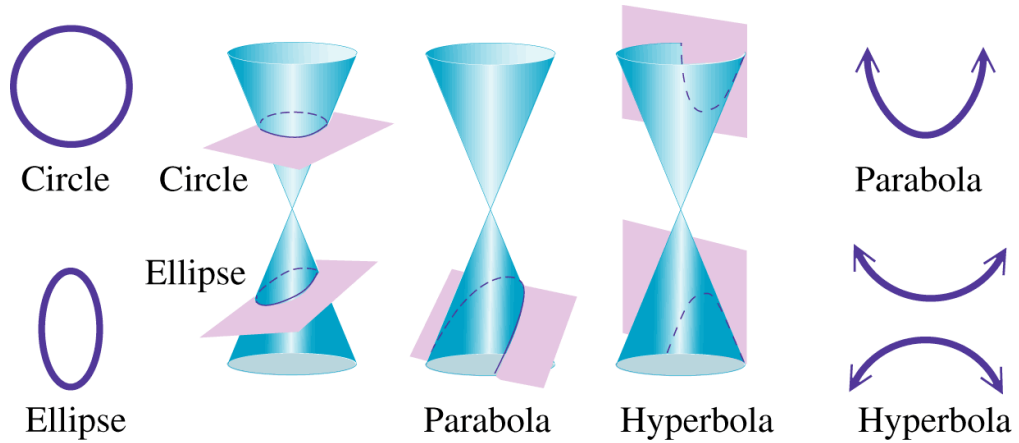
Figure 2.2: Conic sections

The different shapes depend on the *eccentricity* parameter e, thus:

1. Ellipse: $0 < e < 1$

2. Circle: $e = 0$

3. Parabola: $e = 1$

4. Hyperbola: $e > 1$

The most important properties of (ORE) are:

13

- The origin is located at one focus

- θ it is measured from the conic point closest to the focus.

- p determines the size

- e determines the shape

2.5.1 Ellipse

An ellipse is the locus of points the sum of whose distances from two fixed points (*foci*) is constant and equal to two times the *semi-major axis.*
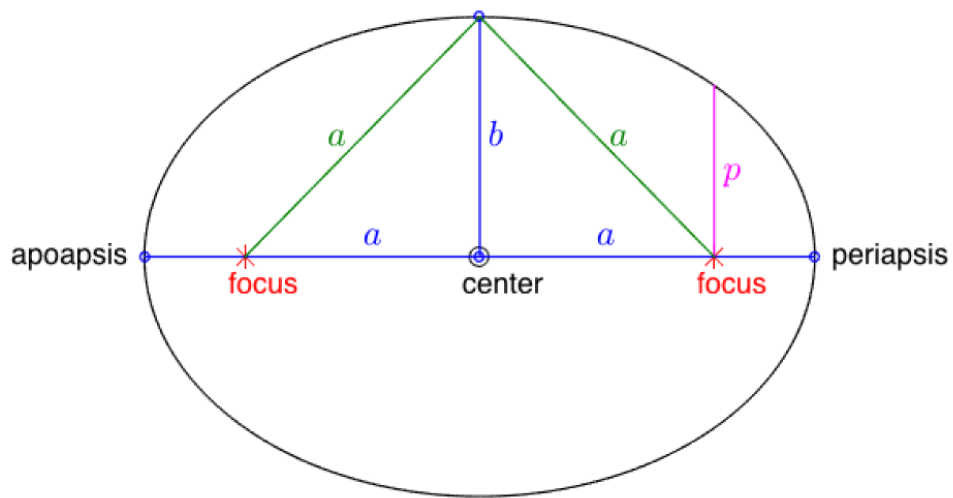
Figure 2.3: Ellipse

Below the most important parameters, quantities and points:

Eccentricity	$0 < e < 1$
Semilatus rectum	$p = \frac{h^2}{\mu}$
Semi-major axis	$a = \frac{p}{1-e^2}$
Semi-minor axis	$b = a\sqrt{1-e^2}$
Distance center-focus	$c = ae$
Total mechanical energy	$\mathcal{E} = -\mu/(2a) < 0$
Velocity (Vis-viva equation)	$v = \sqrt{2\mu/r - \mu/a}$
Periapsis	$\theta = 0, \ r_p = \frac{p}{1+e}$
Apoapsis	$\theta = \pi, \ r_a = \frac{p}{1-e}$

Table 2.1: Ellipse parameters

Note that the two *apsides*, i.e. *periapsis* and *apoapsis*, take different names depending on the context. In particular:

− Perihelion and Aphelion for a body orbiting around the Sun

− Perigee and Apogee for a body orbiting around the Earth

2.5.2 Circle

A circle is the locus of points that are at a given distance (radius) from a given point, the centre. It is also a kind of ellipse in which the two *foci* are coincident, the *eccentricity* is zero, the *semi-major* and *semi-minor* axes are equal and coincident with the *semilatus rectum*, i.e. it coincides with the radius (see (ORE)).

Using (ORE) and substituting $e = 0$, yields:

$$r = p = \frac{h^2}{\mu} = \text{const} \tag{2.15}$$

since $h = rv = \text{const}$, that means that r and v are coplanar, we can substitute it in (2.15) and solve it for v, obtaining then the velocity of a circular orbit:

$$v = \sqrt{\frac{\mu}{r}} = \text{const} \tag{2.16}$$

The total mechanical energy can be derived from the elliptical one, knowing that $a = r$. Thus $\mathcal{E} = -\mu/(2r) < 0$

2.5.3 Parabola

A parabola is the locus of points whose distance from a fixed point (*focus*) is equal to the distance from a fixed line (*directrix*).
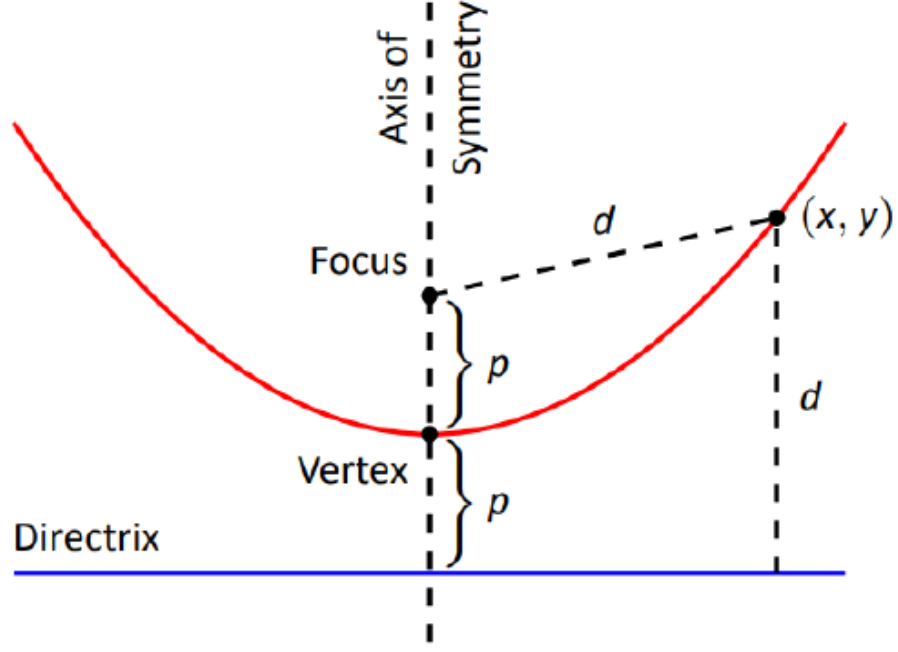
Figure 2.4: Parabola

Below the most important parameters, quantities and points:

Eccentricity	$e = 1$
Semilatus rectum	$p = \frac{h^2}{\mu}$
Semi-major axis	$a \to \infty$
Total mechanical energy	$\mathcal{E} \to 0$
Velocity (Escape velocity)	$v_e = \sqrt{2\mu/r}$
Periapsis	$\theta = 0,\ r_p = \frac{p}{2}$
Apoapsis	$\theta = \pi,\ r_a \to \infty$

Table 2.2: Parabola parameters

2.5.4   Hyperbola

An hyperbola is the locus of points the difference of whose distances from two fixed points (*foci*) is constant and equal to minus two times the *semi-major axis.*
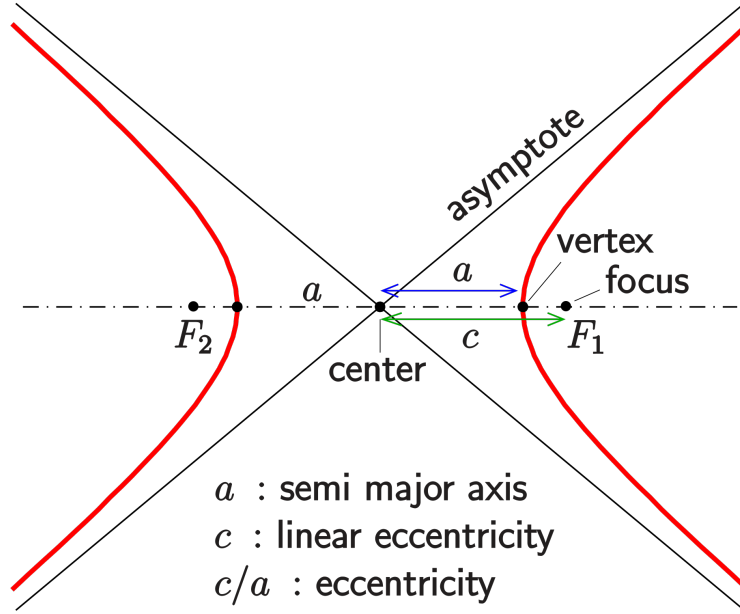
Figure 2.5: Hyperbola

Below the most important parameters and quantities:

Eccentricity	$e > 1$
Semilatus rectum	$p = \frac{h^2}{\mu}$
Semi-major axis	$a = \frac{p}{1-e^2} < 0$
Velocity (Excess velocity)	$v_\infty = \sqrt{\mu/|a|}$
Total mechanical energy	$\mathcal{E} = v_\infty^2/2 > 0$
Angle between asymptotes	$\theta_\infty = \arccos(-1/e)$

Table 2.3: Hyperbola parameters

2.6 Reference frames

Depending on the kind of application/mission, it is more convenient to use one reference frame than another. The most used in aerospace applications are:

1. LVLH: Local Vertical Local Horizontal frame

2. LORF: Local Orbit frame

3. PF: Perifocal (Perigee) frame

4. GE: Geocentric Equatorial frame

5. RIC: Radial In-track Cross-track frame

2.6.1 LVLH

It is a non inertial reference frame because its origin is on a body P_1 subject to accelerated motion. Its unit vectors are defined as follow:

* $\mathbf{l_3}$ (Local Vertical): defined along the direction $P_0 \rightarrow P_1$, on the orbit plane;

* $\mathbf{l_1}$ (Local Horizontal): perpendicular to $\mathbf{l_3}$, on the orbit plane, sign concordant with the orbital velocity;

* $\mathbf{l_2} = \mathbf{l_3} \times \mathbf{l_1}$ (Orbit pole): perpendicular to the orbit plane.
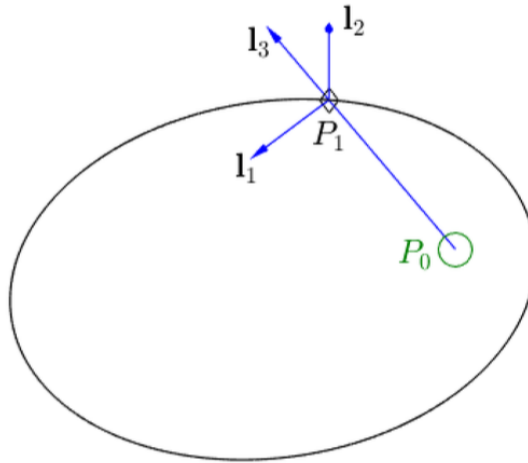
Figure 2.6: LVLH

2.6.2   LORF

It is a non inertial reference frame too. Its unit vectors are defined as follows:

* $\mathbf{o_1}$: instantaneous normalized velocity, on the orbit plane, tangent to the orbit;

* $\mathbf{o_2} = \mathbf{l_2}$ (Orbit pole): perpendicular to the orbit plane;

* $\mathbf{o_3} = \mathbf{o_1} \times \mathbf{o_2}$: on the orbit plane.
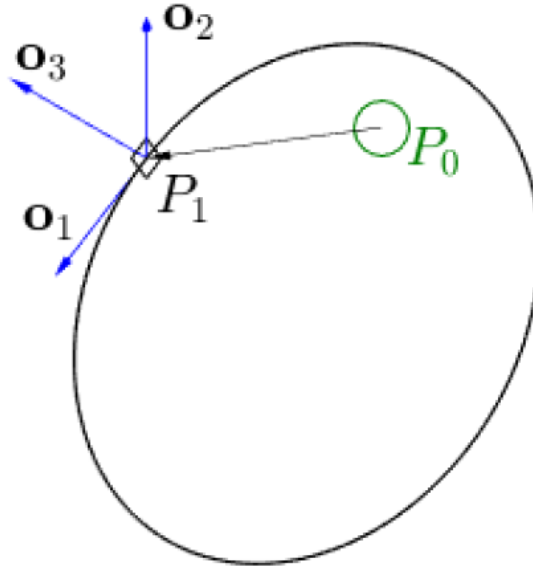
Figure 2.7: LORF

2.6.3   PF

It is a inertial reference frame, with origin on body P_0, because the axes do not rotate relative to the fixed stars. Its unit vectors are defined as follows:

* $\mathbf{p_1} = \mathbf{e}/e$: eccentricity unit vector passing through the periapsis, on the orbit plane;

* $\mathbf{p_3} = \mathbf{o_2} = \mathbf{l_2}$ (Orbit pole): perpendicular to the orbit plane;

* $\mathbf{p_2} = \mathbf{p_3} \times \mathbf{p_1}$: on the orbit plane.
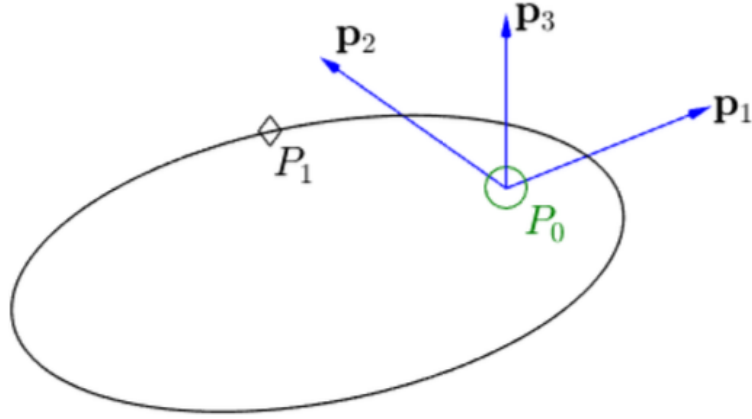
Figure 2.8: PF

2.6.4 GE

It is a inertial reference frame, with origin at Earth CoM, because the axes do not rotate relative to the fixed stars and then they don't rotate with the Earth. It is also known as ECI, Earth-Centered Inertial reference frame. Its unit vectors are defined as follows:

* $\hat{\mathbf{I}}$: Earth $\rightarrow$ Sun direction, 1st day of spring (vernal equinox);

* $\hat{\mathbf{K}}$: polar rotation axis;

* $\hat{\mathbf{J}} = \hat{\mathbf{K}} \times \hat{\mathbf{I}}$: on the equatorial plane.
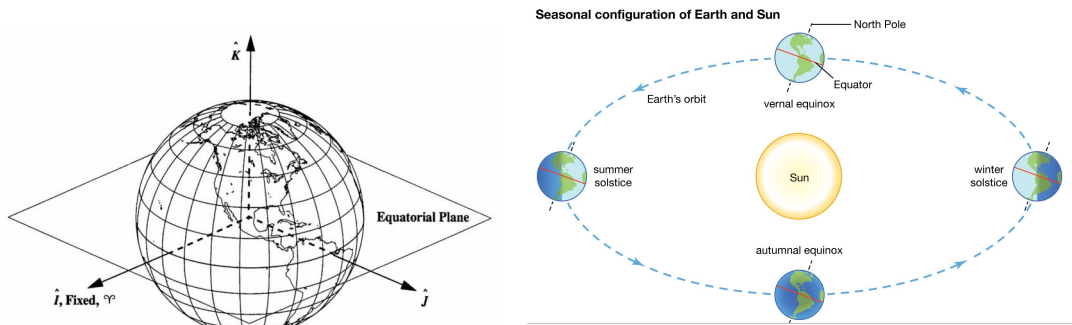
Figure 2.9: GE and seasonal configuration Earth/Sun

2.6.5   RIC

It is a non inertial reference frame, with origin on the center of the S/C. Its unit vectors are defined as follows:

* $\hat{\mathbf{R}}$ (Radial): Vector pointing in the direction of the Spacecraft's position vector;

* $\hat{\mathbf{W}}$ (Cross-track): Vector pointing in the direction normal to the orbit plane (along the angular momentum vector);

* $\hat{\mathbf{S}}$ (In-track): Vector perpendicular to the Radial and Cross-track axes, forming a right-handed coordinate system.
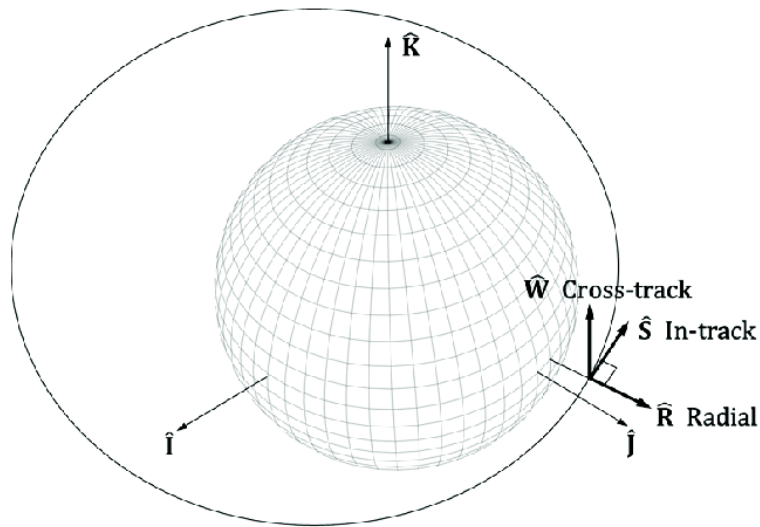
Figure 2.10: RIC

2.7 Keplerian orbital elements

In astronomy and orbital mechanics, it's more common and intuitive to use other parameterizations to describe the S/C dynamics. In fact, it can be uniquely determined by a set of six orbital parameters known as *Keplerian orbital elements*. As shown in the following figure, these elements are:
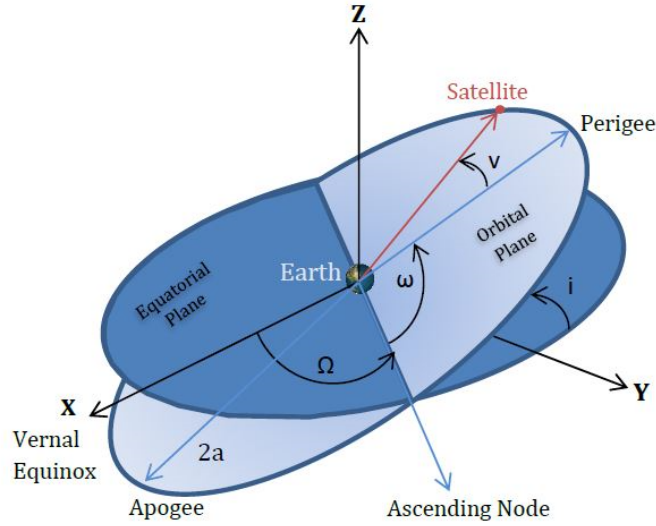
Figure 2.11: Keplerian Orbital Elements

- **Semimajor axis** a: describes the size of orbit ellipse

- **Eccentricity** e: describes the shape of orbit ellipse

- **Inclination** i: the angle between the orbit plane and Earth's equatorial plane

- **Right ascension of ascending node** Ω: the angle from the vernal equinox to the ascending node (intersection between the orbital and the equatorial plane)

- **Argument of perigee** ω: the angle from the ascending node to the eccentricity vector measured in the direction of satellite's motion

- **True anomaly** $\nu \equiv \theta$: indicates the position of the satellite in its orbit

Below a table in which are reported the most important characteristics of these elements:

Name	Element	Range of values	Undefined
Semimajor axis	a	Depends on the conic section	Never
Eccentricity	e	$e = 0,\ 0 < e < 1$	Never
Inclination	i	$0 \leq i \leq 180°$	Never
Right ascension of the ascending node	Ω	$0 \leq \Omega \leq 360°$	When $i = 0$ or $180°$ (Equatorial orbit)
Argument of perigee	ω	$0 \leq \omega \leq 360°$	When $i = 0$ or $180°$ (Equatorial orbit) or $e = 0$ (Circular orbit)
True anomaly	ν	$0 \leq \nu \leq 360°$	When $e = 0$ (Circular orbit)

Table 2.4: Keplerian Orbital Elements

As reported in [8], since the *Keplerian orbital elements* are strictly related to the S/C dynamics expressed in position $\mathbf{r}$ and velocity $\mathbf{v}$, it is possible to derive from each other with some mathematical transformations.

2.7.1 From Position, Velocity to Keplerian Orbital Elements

Suppose the S/C position $\mathbf{r}$ and velocity $\mathbf{v}$ are known and expressed in the GE frame. The following quantities can be computed:

$$\mathbf{h} = \mathbf{r} \times \mathbf{v}, \quad \mathbf{e} = \frac{1}{\mu}\mathbf{v} \times \mathbf{h} - \frac{\mathbf{r}}{r}, \quad \hat{\mathbf{I}}' = \hat{\mathbf{K}} \times (\mathbf{h}/h) \tag{2.17}$$

The 6 *Keplerian orbital elements* can be obtained as follows:

$$\begin{aligned} a = h^2/\left(\mu\left(1 - e^2\right)\right), \quad & e = |\mathbf{e}|, & \cos i = \hat{\mathbf{K}} \cdot \mathbf{h}/h \\ \cos\omega = \hat{\mathbf{I}}' \cdot \mathbf{e}/e, \quad & \cos\Omega = \hat{\mathbf{I}} \cdot \hat{\mathbf{I}}', & \cos\theta = \mathbf{r} \cdot \mathbf{e}/(re) \end{aligned} \tag{2.18}$$

An other useful parameter is the period $P = 2\pi\sqrt{\frac{a^3}{\mu}}$.

23

2.7.2 From Keplerian Orbital Elements to Position, Velocity

Suppose the 6 *Keplerian orbital elements* are known. The *semilatus rectum* and the *radial position* can be computed as:

$$p = a\left(1 - e^2\right), \quad r = \frac{p}{1 + e\cos\theta}. \tag{2.19}$$

The S/C position and velocity, expressed in PF frame, are given by:

$$\mathbf{r} = \begin{bmatrix} r\cos\theta \\ r\sin\theta \\ 0 \end{bmatrix}, \quad \mathbf{v} = \begin{bmatrix} -\sqrt{\mu/p}\sin\theta \\ \sqrt{\mu/p}(e + \cos\theta) \\ 0 \end{bmatrix} \tag{2.20}$$

If we want to express these quantities in a GE frame, we can use the rotation matrix $\mathbf{T}_{313}(\Omega, i, \omega)$, defined as combination of three elementary rotation matrices:

$$\mathbf{T}_3(\Omega) = \begin{bmatrix} \cos\Omega & -\sin\Omega & 0 \\ \sin\Omega & \cos\Omega & 0 \\ 0 & 0 & 1 \end{bmatrix}$$

$$\mathbf{T}_1(i) = \begin{bmatrix} 1 & 0 & 0 \\ 0 & \cos i & -\sin i \\ 0 & \sin i & \cos i \end{bmatrix} \tag{2.21}$$

$$\mathbf{T}_3(\omega) = \begin{bmatrix} \cos\omega & -\sin\omega & 0 \\ \sin\omega & \cos\omega & 0 \\ 0 & 0 & 1 \end{bmatrix}$$

since $\mathbf{T}_{313}(\Omega, i, \omega) \doteq \mathbf{T}_3(\Omega)\mathbf{T}_1(i)\mathbf{T}_3(\omega)$, we have:

$$\mathbf{T}_{313}(\Omega, i, \omega) = \begin{bmatrix} c\Omega c\omega - s\Omega cis\omega & -c\Omega s\omega - s\Omega cic\omega & s\Omega si \\ s\Omega c\omega + c\Omega cis\omega & -s\Omega s\omega + c\Omega cic\omega & -c\Omega si \\ sis\omega & sic\omega & ci \end{bmatrix} \tag{2.22}$$

where $c = \cos(\cdot)$ and $s = \sin(\cdot)$. If we want to express position and velocity in a PF frame starting from a GE frame, it is sufficient to use the following rotation matrix $\mathbf{T}_{313}(-\omega, -i, -\Omega) \doteq \mathbf{T}_3(-\omega)\mathbf{T}_1(-i)\mathbf{T}_3(-\Omega)$.

2.8 Modified Equinoctial orbital elements

As can be noticed in table 2.4, when the orbit is circular and/or equatorial some of the *Keplerian orbital elements* are undefined and then we incur in singularities. In order to solve this problem, a new set of orbital elements is defined, known as *Modified equinoctial orbital elements*. As stated in [9], they are valid for circular, elliptic, and hyperbolic orbits and exhibit no singularity for zero eccentricity and orbital inclinations equal to 0 and 90 degrees. However, two of the components are singular for an orbital inclination of 180 degrees (not of interest from thesis project point of view).

2.8.1 Relationship between MEOE and KOE

$$p = a \left(1 - e^2\right)$$

$$f = e \cos(\omega + \Omega)$$

$$g = e \sin(\omega + \Omega)$$

$$h = \tan(i/2) \cos \Omega$$

$$k = \tan(i/2) \sin \Omega$$

$$L = \Omega + \omega + \theta$$

$$(2.23)$$

where L is the true longitude, that is, as stated in [10], the ecliptic longitude at which an orbiting body could actually be found if its inclination were zero. Together with the inclination and the ascending node, the true longitude can tell us the precise direction from the central object at which the body would be located at a particular time.

2.8.2 Relationship between KOE and MEOE

$$a = \frac{p}{1 - f^2 - g^2}$$

$$e = \sqrt{f^2 + g^2}$$

$$i = 2\tan^{-1}\left(\sqrt{h^2 + k^2}\right) = \tan^{-1}\left(2\sqrt{h^2 + k^2}, 1 - h^2 - k^2\right)$$

$$\omega = \tan^{-1}(g/f) - \tan^{-1}(k/h) = \tan^{-1}(gh - fk, fh + gk)$$

$$\Omega = \tan^{-1}(k, h)$$

$$\theta = L - (\Omega + \omega) = L - \tan^{-1}(g/f)$$

(2.24)

where $tan^{-1}(a, b)$ indicates a four quadrant inverse tangent.

2.8.3 Relationship between ECI Position, Velocity and MEOE

$$\mathbf{r} = \begin{bmatrix} \frac{r}{s^2}\left(\cos L + \alpha^2 \cos L + 2hk\sin L\right) \\ \frac{r}{s^2}\left(\sin L - \alpha^2 \sin L + 2hk\cos L\right) \\ \frac{2r}{s^2}(h\sin L - k\cos L) \end{bmatrix}$$

$$\mathbf{v} = \begin{bmatrix} -\frac{1}{s^2}\sqrt{\frac{\mu}{p}}\left(\sin L + \alpha^2 \sin L - 2hk\cos L + g - 2fhk + \alpha^2 g\right) \\ -\frac{1}{s^2}\sqrt{\frac{\mu}{p}}\left(-\cos L + \alpha^2 \cos L + 2hk\sin L - f + 2ghk + \alpha^2 f\right) \\ \frac{2}{s^2}\sqrt{\frac{\mu}{p}}(h\cos L + k\sin L + fh + gk) \end{bmatrix}$$

(2.25)

where

$$\alpha^2 = h^2 - k^2$$
$$s^2 = 1 + h^2 + k^2$$
$$r = \frac{p}{w}$$
$$w = 1 + f\cos L + g\sin L$$

26

2.8.4   Modified equinoctial form of the orbital equations of motion

The orbital dynamics can be expressed, using the *Modified equinoctial orbital elements*, as a set of six first-order differential equations:

$$\dot{p} = \frac{dp}{dt} = \frac{2p}{w}\sqrt{\frac{p}{\mu}}\Delta_t$$

$$\dot{f} = \frac{df}{dt} = \sqrt{\frac{p}{\mu}}\left[\Delta_r \sin L + [(w+1)\cos L + f]\frac{\Delta_t}{w} - (h\sin L - k\cos L)\frac{g\Delta_n}{w}\right]$$

$$\dot{g} = \frac{dg}{dt} = \sqrt{\frac{p}{\mu}}\left[-\Delta_r \cos L + [(w+1)\sin L + g]\frac{\Delta_t}{w} + (h\sin L - k\cos L)\frac{g\Delta_n}{w}\right]$$

$$\dot{h} = \frac{dh}{dt} = \sqrt{\frac{p}{\mu}}\frac{s^2\Delta_n}{2w}\cos L$$

$$\dot{k} = \frac{dk}{dt} = \sqrt{\frac{p}{\mu}}\frac{s^2\Delta_n}{2w}\sin L$$

$$\dot{L} = \frac{dL}{dt} = \sqrt{\mu p}\left(\frac{w}{p}\right)^2 + \frac{1}{w}\sqrt{\frac{p}{\mu}}(h\sin L - k\cos L)\Delta_n$$

$$(2.26)$$

where $\Delta_r, \Delta_t, \Delta_n$ denote the *non-two-body* perturbations in the radial, tangential and normal axes. The radial direction is along the geocentric radius vector of the S/C measured positive away from the Earth's centre, the tangential direction is perpendicular to this radius vector measured positive in the direction of orbital motion, and the normal direction is positive along the angular momentum vector of the S/C's orbit. As can be seen, if the motion remains unaltered, i.e. $\Delta_r = \Delta_t = \Delta_n = 0$, the first five equations of motion are simply $\dot{p} = \dot{f} = \dot{g} = \dot{h} = \dot{k} = 0$, that is $p = f = g = h = k = \text{const}$.

2.9 Initial and target orbit definition through MEOE

The initial orbit is LEO, circular ($e = 0$) and equatorial ($i = 0$). It is characterized by the following *Modified equinoctial orbital elements*:

- $p = 6771$ km

- $f = 0$

- $g = 0$

- $h = 0$

- $k = 0$

The target orbit is GEO, circular ($e = 0$) and equatorial ($i = 0$). It is characterized by the following *Modified equinoctial orbital elements*:

- $p = 42164$ km

- $f = 0$

- $g = 0$

- $h = 0$

- $k = 0$

As can be noticed from (2.23), if the eccentricity e is equal to zero, then p coincides with the semimajor axis a. The true longitude L has not been defined neither for initial orbit nor for target orbit because we are not interested about the S/C exact position along the orbit.

Chapter 3

Nonlinear Model Predictive Control

The aim of this chapter is to provide an overview about the history of Model Predictive Control, the strategy, the properties and the mathematical formulation, highlighting the differences between the linear and nonlinear approaches and between the advantages and drawbacks.

3.1 History of Model Predictive Control

The development of modern control concepts can be traced back to the work of Kalman in the early 1960s with the linear quadratic regulator (LQR) designed to minimize an unconstrained quadratic objective function of states and inputs [11]. This control technique had no so relevant impact in the industrial word of that age, because of absence of constraints in its formulation, the nonlinearities of the real systems and distrust of optimal control concept. Starting from 1970s, model predictive control strategy became popular in industrial processes, thanks to people like Richalet (1978) that presented Model Predictive Heuristic Control (later known as Model Algorithmic Control (MAC)) and Cutler and Ramaker (1980) with Dynamic Matrix Control (DMC). The idea behind these strategies was the same, i.e. using a dynamic model of the process to predict the effect of the future control actions, which were determined by minimizing the predicted error, based on a repeated optimization at each sampling time with new data coming from the process. These formulations were algorithmic, heuristic and not automatically stabilizing, because it wasn't yet strong theoretical studies about stability. MPC is now suited for controlling rapid dynamical systems such as automotive systems, aerospace systems, chemical processes, robotics, and biomedical devices, following years of research and thanks to technical advances in the areas of optimization

algorithms and hardware processing speed. The following are the fundamental concepts underlying the various predictive control family approaches: [12] :

- Use of a model explicitly to anticipate process output at future time instants (horizon)

- Development of a control sequence that minimises an objective function

- Receding strategy, in which the horizon is shifted forward at each moment by applying the first control signal in the sequence computed at each step.

3.2   MPC advantages and drawbacks

The principal advantages of this approach are the following [12]:

- It may be used to regulate a wide range of processes, from those with relatively simple dynamics to those with more complex dynamics, such as systems with extended delay periods, nonminimum phase, or unstable dynamics.

- SISO and MIMO are both simply handled.

- It features built-in compensation for downtime.

- It introduces feed forward control action to compensate for quantifiable disturbances.

- The resultant controller is a simple control law.

- Its application to the treatment of constraints is theoretically straightforward, and it may be included systematically during the design process.

As other control techniques, it has drawbacks and limitations. The most important need is the availability of a suitable process model. The more the model is far from the real plant, the more the control law generated will be less accurate. An other drawback is the high computational cost since all the computations are made online and at each sampling time. When constraints are included the computational cost becomes even higher.

3.3 NMPC advantages and drawbacks

In some cases the linear model predictive approach is not sufficient to control systems that have highly nonlinear dynamics and that include linear or nonlinear constraints. For this reason, a new version of the model predictive strategy that use a nonlinear model for the prediction have to be take into account, its name is Nonlinear Model Predictive Control (NMPC). Below the main advantages and drawbacks [8]:

Advantages

- General and flexible: complex MIMO systems

- Intuitive formulation, based on optimality concepts

- Constraints and input saturation accounted for

- Efficient management of the performance/input activity trade-off

- Optimal trajectories (over a finite time interval)

- Unified computation of optimal trajectory and control law (in aerospace field unifies the Navigation and Control part of GNC)

Drawbacks

- High on-line computational cost

- Possible local minima in the optimization problem

- Problems in the case unstable zero-dynamics

3.4 MPC vs NMPC

The main differences between the two strategies concern three macro areas, i.e. the optimization problem, the plant of the system to be controlled and the constraints. The following table lists them:

Strategy	Optimization	Plant	Constraints
MPC	Considering convex constraints, the optimization problem is convex, this guarantees global optimum	Requires linearization (Jacobian linearization) of the dynamics at a given working point or along a trajectory. The last one can more complicated, especially in trajectory tracking problems	Requires constraint convexification and this can be complicated
NMPC	Only local optima can be found in general, since the optimization problem is non-convex	Can use directly a nonlinear model	Can use simple inequalities to describe constraints

Table 3.1: MPC vs NMPC

3.5 NMPC strategy

In general, the model predictive control problem is defined as an on-line solution to a finite horizon open-loop optimum control problem including its dynamics and states and control input as constraints. This strategy is well summarized in the figure below:
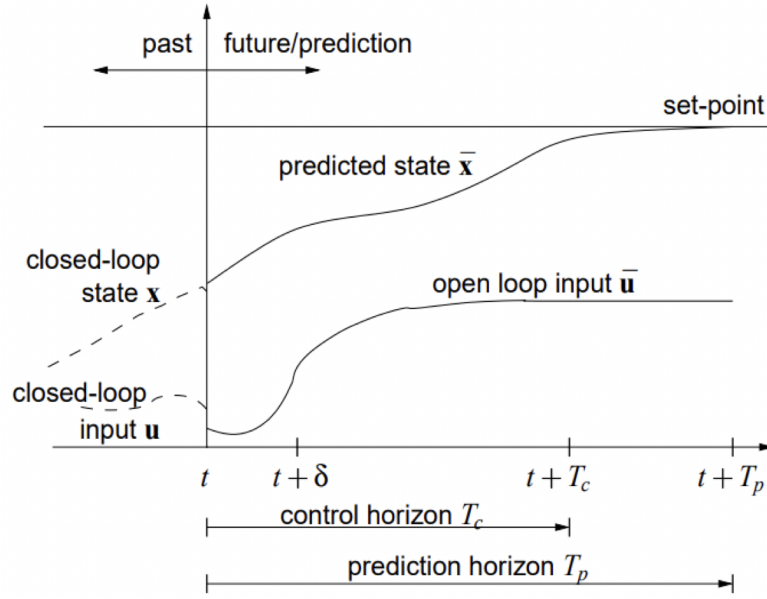
Figure 3.1: NMPC strategy

Based on the measurements collected at time t, the controller:

1. Predicts the system's future dynamic behaviour across a **Prediction horizon** T_p

2. Determines the command signal u so that a preset open-loop performance cost functional is optimized across a **Control horizon** $T_c \leq T_p$, in order to produce the best prediction, i.e. the prediction closest to the intended behaviour.

In a perfect world, as reported in [13], with no disturbances, no model-plant mismatch, and limitless prediction horizons, the input function discovered at the initial time could be applied to the system for all times greater or equal to the initial one. In general, however, this is not achievable since the true real-world system behaviour differs from the estimated one. Then, in order to implement the acquired open-loop modified input function just till the next measurement becomes available, some feedback mechanism must be included. The time interval between measurements is assumed to be constant and equal to δ; this number, also denoted as T_s, is referred to as **Sampling time**. The entire approach (prediction and optimization) is repeated using the new measurement at time $t + \delta$ in order to develop a novel input function with shifting forward control and prediction horizons. Furthermore, the computation of the command input based on system behaviour, at each time step, enables for the insertion of state and input limits.

3.6   Basic structure

The algorithm basic structure to be implemented is based on the following block scheme:
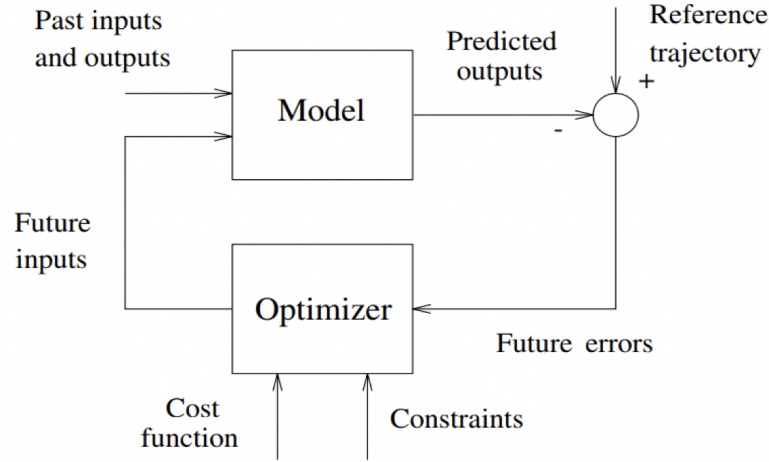
Figure 3.2: NMPC basic structure

Model

The model, as shown in the image above, is used to estimate future plant outputs based on previous and present values as well as the indicated ideal future control actions. The chosen model must then be able to properly represent the dynamics of the process in order to offer an accurate prediction of the behaviour while also being straightforward to apply. A bad and incomplete model will cause the algorithm to create an ineffective control action. It is separated into two parts: process models and disturbance models. The former can be stated in a variety of ways, but the state space representation is the most commonly employed, particularly in the academic research community, since it allows for a relatively easy controller derivation, even in the multi-variable situation. The latter considers the impact of non-measurable inputs, noise, and model mistakes.

Optimizer

The optimizer's goal is to offer control actions by minimising a cost function that also takes into consideration the presence of system constraints. If the cost function is quadratic, the minimum can be calculated as an explicit (linear) function of previous inputs and outputs as well as the future reference trajectory. Instead,

when inequality restrictions are included, the cost function becomes more complicated and has a substantially greater computing cost. The optimizer's control action is such that it pushes the process to meet the required specifications while also meeting the a-priori constraints.

3.7 Primal Control problem formulation

Let consider a generic nonlinear system described by a state space representation, as stated in [13]:

$$\begin{aligned} \dot{x} &= f(x, u) \\ y &= h(x, u) \end{aligned} \tag{3.1}$$

where $x \in \mathbb{R}^n$ is the state, $u \in \mathbb{R}^{n_u}$ is the command input and $y \in \mathbb{R}^{n_y}$ is the output of the system.

Assuming that the state is measured on-line, with a sampling time T_s, then the measurements will be: $x(t_k)$ with $t_k = T_s k$ for $k = 0, 1, \ldots$ If this assumption does not hold, an observer must be designed (e.g. a Kalman filter). Furthermore let's assume that the output y coincides with the state x

Let's now analyse deeply the two main key operations in the NMPC strategy, i.e. prediction and optimization.

3.7.1 Prediction

According to [8] at time t, integration of (3.1) or a model of it yields a prediction of the state and output throughout the interval $[t, t + T_p]$. In general, at a given instant of time [t, t+ Tp], the predicted output $\hat{y}$ is a function of the starting state $x(t)$ and the input signal $u(t : \tau)$ (that is, the input specified in the interval $[t, \tau]$):

$$\hat{y}(\tau) \equiv \hat{y}(\tau, x(t), u(t : \tau))$$

As illustrated in Figure 3.1, u is an open-loop input since its value in the range $[t, t + T_p]$ is independent of the value assumed by the state x in that interval.

3.7.2 Optimization

The goal of this control strategy is to create an input signal $u^*(t : \tau)$ at each sample time T_s such that the prediction $\hat{y}(\tau) \equiv \hat{y}(\tau, x(t), u^*(t : \tau)) \equiv \hat{y}(u^*(t : \tau))$ exhibits the expected behaviour for $\tau \in [t, t + T_p]$. By defining the cost functional, the notion of intended behaviour is expressed:

$$J\left(u\left(t : t + T_p\right)\right) \doteq \int_t^{t+T_p} \left(\|\tilde{y}_p(\tau)\|_Q^2 + \|u(\tau)\|_R^2 \right) d\tau + \|\tilde{y}_p\left(t + T_p\right)\|_P^2 \tag{3.2}$$

where $\|\tilde{y}_p(\tau)\| \doteq r(\tau) - \hat{y}(\tau)$ is the predicted tracking error and $r(\tau) \in \mathbb{R}^{n_y}$ is the tracking reference. The symbol $\| \cdot \|_X$, in the formula above, represent weighted vector norms, and their integrals represent square signal norms.

So, in order to achieve the required behaviour, the input signal $u^*(t : t + T_p)$ is chosen as the one that minimises the cost functional $J(u(t : t + T_p))$ at each time $t = t_k$. In other words, it implies reducing the three terms that make it up:

1. $\|\tilde{y}_p(\tau)\|_Q^2$: this is the tracking error norm, which is the difference between the reference signal and the predicted output instant by instant;

2. $\|\tilde{u}(\tau)\|_R^2$: this concept provides for the management of the trade-off between performance and command activity;

3. $\|\tilde{y}_p(t + T_p)\|_P^2$: this expression emphasises the terminal tracking error.

The square weighted norm of a generic vector $v \in \mathbb{R}^n$ is:

$$\|v\|_Q^2 \doteq v^T Q v = \sum_{i=1}^{n} q_i v_i^2, \quad Q = \mathrm{diag}(q_1, \ldots, q_n) \in \mathbb{R}^{n \times n}$$

where $q_i \geq 0$ are the weights of the matrix Q. The values supplied to the matrices Q, R and P are critical for NMPC design since they govern the optimization process. Indeed, depending on these weights, more or less emphasis might be assigned to the minimising of each of the three variables.

One of the most significant benefits of the NMPC technique is the inclusion, during the optimization problem, of limitations on state/output variables (e.g., for barriers or collision avoidance) and on the input variable (e.g. for input saturation).

3.7.3 Mathematical formulation

The overall formulation of the optimization problem, as explained in the following subsections, is as follows:

$$u^*(t : t + T_p) = \arg \min_{u(\cdot)} J(u(t : t + Tp))$$

subject to:

$$\dot{\hat{x}}(\tau) = f(\hat{x}(\tau), u(\tau)), \quad \hat{x}(t) = x(t)$$
$$\hat{y}(\tau) = h(\hat{x}(\tau), u(\tau))$$
$$\hat{x}(\tau) \in X_c, \ \hat{y}(\tau) \in Y_c, \ u(\tau) \in U_c$$
$$u(\tau) = u(t + T_c), \quad \tau \in [t + T_c, t + T_p]$$

where X_C, Y_C and U_C are sets describing possible constraints on the state, output and input, respectively.

As stated in [14], the above optimization problem is numerically not tractable, since $u(\cdot)$ is a continuous-time signal and then the number of decision variables is potentially infinite. So, in case of a numerical solution is needed, an a-priori finite parametrization of the input signal $u(\cdot)$ must be assumed.

At time t, as reported in [13], the open-loop input $u^*(t : t + T_p)$ is the best solution to the minimization problem; it is affected by $x(t)$ but not by $x(\tau)$, with $\tau > t$. The control then does not undertake any feedback action that may enhance accuracy or minimise errors and disturbance effects if this signal is applied over the whole time period $[t, t + T_p]$. The **Receding Horizon Strategy** must be implemented to overcome this open-loop behaviour and create a feedback control algorithm. The following stages describe it:

- At time $t = t_k$, the optimal input $u^*(t : t + T_p)$ is computed via optimization.

- Only the first input value $u(\tau) = u^*(t = t_k)$ is used while the other ones are discarded. It remains constant for $\forall \tau \in [t_k, t_{k+1}]$

- Steps 1 and 2 are repeated for $t = t_{k+1}, t_{k+2}, \ldots$

In this manner, the best input u^* is computed instant by instant. This signal is applied to the process for the duration of T_s. The optimization method then computes a new optimum input depending on the actual state. As seen in Figure 3.3, this method results in a closed loop control; the controller is able to sense the state development at each T_s and then reacting to potential uncertainty errors and unpredicted disturbances..
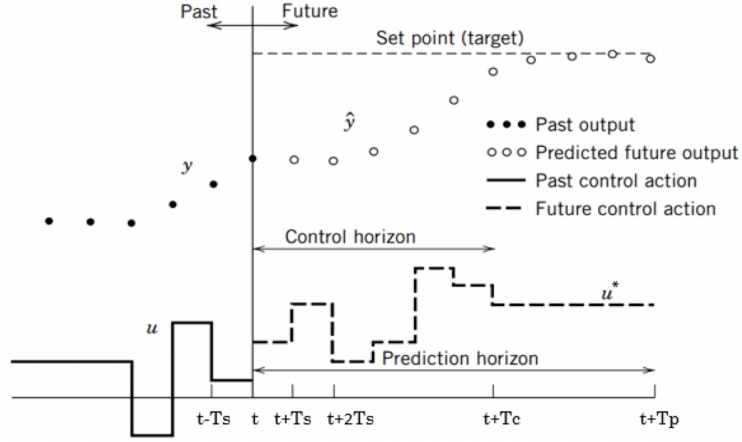
Figure 3.3: NMPC with Receding Horizon Strategy

3.8   Dual Control problem formulation

A dual control problem formulation can be achieved starting from the primal problem and taking advantage of the PMP, i.e. Pontryagin Minimum (or Maximum) Principle, as stated in [7].

The advantage of using this optimization algorithm is mainly due to two factors: first it does not require any a-priori assumption about the control signal parametrization (as happened with the Primal Control problem) and second it allows us to obtain an explicit and analytical equation for the optimal control input $u^*(t)$.

The necessary condition for a control $u(t)$ to be optimal and a trajectory $x(t)$ to be the extremal path is that the Hamiltonian scalar function $H(x(t), u(t), \lambda(t))$ attains its minimum value when $u(t) = u^*(t)$. Keeping implicit the time dependence, the Hamiltonian function is defined as:

$$H(x, u, \lambda) = \Phi(x, u) + \lambda^T (f(x) + g(x)u) \tag{3.3}$$

where λ is the vector of Lagrangian (or co-state) variables and $\Phi(x, u)$ is the integrand function in (3.2), i.e. $\Phi(x, u) = \left(\|\tilde{y}_p(\tau)\|_Q^2 + \|u(\tau)\|_R^2 \right)$. The optimization problem is subject to both the dynamics $\dot{x} = f(x, u) = f(x(t)) + g(x(t))u(t)$ and the dynamics of the co-state variables λ, which evolution is described by the so-called Euler-Lagrange differential equations:

$$\dot{\lambda} = -\nabla_x (H(x, u, \lambda)) \tag{3.4}$$

38

The state and co-state dynamics are the first-order optimality conditions. These latter differential equations must satisfy a set of boundary conditions to be imposed, at the borders of the prediction horizon, both on the state and the co-state. As for the state, at each time $t = t_k$ the value cannot be chosen arbitrarily: the continuity between two successive sampling steps must be ensured, whereas the same continuity condition is no required for the co-states. On the other hand, the λ vector must satisfy the boundary conditions for optimality (see [15]) at the end of prediction horizon. In formulae:

$$\begin{cases} \lambda(t_0)^T + \mu^T \nabla_{x(t_0)} \psi(x) = 0 \\ \lambda(t_F)^T - \nabla_{x(t_F)} \phi(x(t_F)) - u^T \nabla_{x(t_F)} \psi(x) = 0 \end{cases} \tag{3.5}$$

knowing that $\psi(x) = 0 \rightarrow \psi(x) = x(t_0) - x_0 = 0$ is due to the continuity between two consecutive steps and $\phi(x(t_F)) = \|\tilde{y}_p(t + t_P)\|_P^2$ is the terminal cost rate of the functional (3.2). Substituting them in (3.5) and simplifying, we obtain:

$$\begin{cases} \lambda(t_0) = \mu \\ \lambda(t_F) = 2P\tilde{y}_p(t + t_P) \\ x(t_0) = x_0 \end{cases} \tag{3.6}$$

where μ is an auxiliary variable. Note that the first boundary condition will not be taken into account, as explained before. At the end, the dual optimization problem, according to the PMP, can be formulated as follows:

$$u^*(t) = \arg\min_{u(\cdot)} H(x, u, \lambda)$$

subject to

$$\begin{cases} \dot{x} = f(x) + g(x)u \\ \dot{\lambda} = -\nabla_x(H(x, u, \lambda)) \\ \psi(x) = 0 \rightarrow x_0 = x(t_0) \\ \lambda(t_F) = 2P\tilde{y}_p(t + t_P) \\ x \in X_C , \ u \in U_C \end{cases} \tag{3.7}$$

which is equivalent to solve the equation:

$$\nabla_{u(\cdot)} H(x, u, \lambda) = 0 \tag{3.8}$$

In the case of affine-in-the-input systems, the solution of (3.7), over the prediction horizon, has the following general form:

$$u^*(\tau) = -\mathbf{R}^{-1}\lambda(\tau)^T g(x(\tau)) \tag{3.9}$$

39

where $\boldsymbol{R}$ is the diagonal, constant, square and full rank weight matrix. Since the receding control horizon strategy is adopted, only the first sample of $u^*(\tau)$ is applied to the plant and the remainder of the solution is discarded.

In summary, the (3.1) jointly with the (3.4) and the boundary conditions in (3.6) represent a TPBVP, i.e. Two-Points Boundary Value Problem, to be solved over the prediction horizon $[t, t + T_p]$. The TPBVP solution provides the λ (i.e. the gains) of the explicit control law (3.9), hence, turning the optimal control problem into a standard TPBVP. Note that, (3.1), (3.4), and (3.6) are the Karush-Kuhn-Tucker (KKT) conditions of the dual optimization problem.

3.9 NMPC design

As depicted in Figure 3.4, the NMPC method may be implemented as one or more MATLAB functions that are used and linked into the Simulink block scheme.
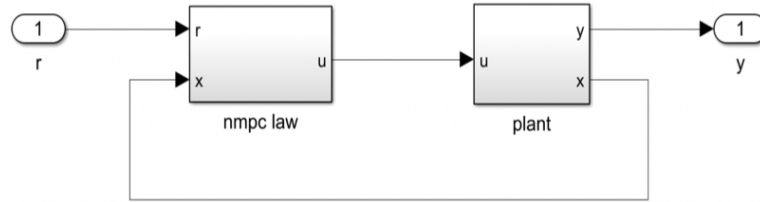
Figure 3.4: NMPC block scheme

The plant block describes the system in detail using the state space representation provided in the equations (3.1). Instead, the NMPC law's model, which is required for prediction and optimization operations, is an approximation of (3.1):

$$
\begin{aligned}
\dot{\hat{x}} &= \hat{f}(\hat{x}, u) \\
\hat{y} &= \hat{h}(\hat{x}, u)
\end{aligned}
\tag{3.10}
$$

where $\hat{f}$ and $\hat{h}$ are approximations of the f and h functions, respectively. It is essential to adopt an approximation model that:

- Simplifies the system description: this is crucial for improving the prediction and optimization algorithm's velocity.

- Does not overlook the key traits of its dynamics.

3.9.1 Parameters choice

The design step entails doing a trial and error method in simulation on the NMPC parameters in order to produce a configuration that can optimise performance while minimising the complexity of the control algorithm. These parameters are the sampling time T_s, the prediction horizon T_p, the control horizon T_c, the number of parametrization parameters m, and the weight matrices.

1. **Sampling time** T_s is the sample time at which the controller conducts the control algorithm. In many cases, this parameter is fixed and cannot be changed; it is determined by the hardware that houses the controller. When its design is accessible, the option must be a trade-off between a sufficiently tiny value to cope with plant dynamics (according to the Nyquist-Shannon sampling theorem) and a sufficiently large number to prevent numerical difficulties and delayed processing.

2. **Prediction and control horizon** The Prediction Horizon T_p defines how far into the future the controller is able to predict. In this situation, the designer must choose a trade-off between a sufficiently big number to improve closed-loop stability and a sufficiently small value to prevent compromising short-time tracking accuracy. T_c, i.e. the Control Horizon, is the time after which the input signal is supposed to be constant. In other words, it tells the controller how many time intervals along the prediction horizon it may adjust the input to achieve the desired behaviour. Then, a short control horizon requires few computations for optimization, whereas a bigger value defines an improvement in speed but an increase in algorithm complexity. When using a polynomial parametrization, it is usually best to specify $T_c = T_p$; otherwise, $T_c = T_s$..

3. **Number of parametrization parameters** The parametrization procedure converts an infinite-dimensional space into one of limited dimension equal to m. It was used to solve the problem of minimising a function with regard to an infinitely large vector, i.e. the input signal $u(\cdot)$. In general, the smaller the parameter m, the fewer the decision variables involved in the optimization, and hence the lower the algorithm's complexity. Furthermore, a small number of parameters is sufficient to achieve good control performance. For these reasons, $m = 1$ is commonly selected.

4. **Weight matrices** The optimization process, that is, the minimization of the cost functional J, may be governed and managed by using three diagonal square matrices, known as weight matrices. Indeed, by modifying each diagonal member of these matrices, a good trade-off between performance and command activity may be found. More specifically:

- Q is connected to tracking error minimization at each sampling time, and it then governs system state optimization;

- P is exclusively connected to the last term of tracking error minimization, and it then governs the system output optimization;

- R is connected to command effort minimization and then governs input optimization.

As an example, we can consider a generic matrix K defined as

$$K = \begin{bmatrix} k_{11} & 0 & \cdots & 0 \\ 0 & k_{22} & \cdots & 0 \\ \vdots & \vdots & \ddots & \vdots \\ 0 & 0 & \cdots & k_{nn} \end{bmatrix}$$

where n is the system order. Each diagonal element assigns a weight (or penalty) to the related state variable in order to reduce it. The greater the weight value, the greater the significance of the variable throughout the optimization process.

The following technique may be used to choose the initial matrix values before modifying the weights through trial and error tuning based on multiple simulations:

$$Q_{ii} = \begin{cases} 1 & \text{in the presence of requirements on } x_i \\ 0 & \text{otherwise} \end{cases}$$

$$P_{ii} = \begin{cases} 1 & \text{in the presence of requirements on } y_i \\ 0 & \text{otherwise} \end{cases}$$

$$R_{ii} = \begin{cases} 1 & \text{in the presence of requirements on } u_i \\ 0 & \text{otherwise} \end{cases}$$

Following that, the values of Q_{ii}, P_{ii} and R_{ii} may be adjusted based on the simulation outputs and system specifications, understanding that:

- A rise in Q_{ii} and P_{ii} causes a drop in x_i and y_i energy and, as a result, a decrease in oscillations and converging time;

- A rise in R_{ii} causes a drop in u_i energy, which leads to a decrease in command effort and fuel consumption.

Chapter 4

Mission scenario and propulsion systems

This chapter describes the exact mission situation and the approaches utilised to accomplish autonomous guidance and control. At the end a brief discussion will concern the main propulsion technologies, used for orbital maneuvers.

4.1 Mission scenario description

The aim of the thesis, as explained in Chapter 1, is to develop a control algorithm able to transfer autonomously a satellite from a nominal initial LEO orbit to a GEO target orbit.
To obtain the autonomous guidance the strategy used is based on the Pontryagin NMPC approach (as reported in Chapter 3). It enables us to optimise the many manoeuvres to be done in order to achieve the autonomous mission and, moreover, to obtain an explicit control law. In particular, it provides a command input for forcing the satellite to follow the optimal trajectory.

4.2 NMPC for guidance and control

As we will analyze deeply, the autonomous guidance consists of a series of dense transfer spirals orbits, with the same inclinations i, around the Earth until the target/final orbit is reached. When dealing with orbital manoeuvres, the difficulty is that the idea of impulsive and immediate thrust action, known as ΔV, is just an abstract and theoretical approximation useful for calculating mission budgets and assessing satellite performance. However, in the real conventional aerospace technique, the ideal ΔV must be divided into limited time periods based on real

thruster characteristics, because the latter have physical limits and cannot generate instantaneous thrust. This is a process that determines an intrinsic drop in satellite performance as well as an increase in propellant budget as a result of gravity and misalignment losses. Furthermore, if the procedure for splitting the thrust is inefficient, the losses may grow. Then, a strategy that ensures optimization of the manoeuvre profile must be used. NMPC looks to be a very promising solution for autonomous manoeuvring and, more broadly, for space mission applications. The following are the reasons:

- Determine the optimal solution for the concerning control problem;

- Take into account the high prediction horizon (T_p) and sampling time (T_s);

- Manage the trade-off between performance and command activity effectively;

- Handle complicated linear and nonlinear constraints

- It is able to merge in a single algorithm the guidance and control tasks, reducing remarkably the human effort in operations like the trajectory planning.

The adopted strategy is the autonomous low-thrust one, i.e. it uses a continuous thrust with a lower propellant consumption with respect to the conventional impulsive ones. This can be noticed by the I_{sp}, i.e. the specific impulse, that varies, accordingly to the different propulsion systems used, in a range 3000-8000 s for low-thrust engines and 200-400 s for high-thrust ones.

In the following sections will be analyzed the most important aerospace propulsion systems, with particular focus on the mathematical rocket equation that describes the motion of S/C.

4.3 Space propulsion systems

Any mechanism used to generate thrust, which is the force that propels spacecraft and artificial satellites through air and space, is referred to as a propulsion system. Different propulsion systems create thrust in different ways, but they all use Newton's third rule of motion. As cited in [13], there are three types of space propulsion systems: escape propulsion (from the Earth's surface to orbit), in-space propulsion (in orbit), and deep space propulsion (from orbit to outer space). Those launch vehicles that are currently used for escape propulsion rely on fairly established technology, but considerable technical breakthroughs are expected for in-space and deep space vehicles. Because we are dealing with LEO-GEO orbit movements in this thesis, we shall solely look at in-space propulsion technologies.

4.3.1 Tsiolkovsky rocket equation

The behaviour of a space thruster is similar to that of a rocket: a device that can impart acceleration to itself utilising thrust and expelling a portion of its mass with high velocity may therefore move according to momentum conservation. Tsiolkovsky rocket equation is the mathematical equation that defines vehicle motion based on the aforementioned premise.

In the context depicted in Figure 4.1, this equation may be obtained:
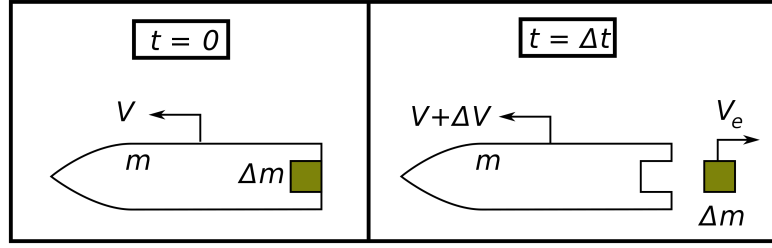
Figure 4.1: (Left) Rocket and propellant system at time $t = 0$. (Right) The system following expulsion of a tiny element Δm of combustion products an instant later.

The propellant ejection causes a momentum variation during Δt, which may be represented using Newton's second law of motion as follows:

$$\sum F_i = \frac{P_2 - P_1}{\Delta t} \tag{4.1}$$

where P_1 is the linear momentum of the rocket at time t:

$$P_1 = (m + \Delta m)V$$

P_2 is the linear momentum of the rocket and expended mass at time $t + \Delta t$:

$$P_2 = m(V + \Delta V) + \Delta m V_e$$

where F_i denotes an external force such as air drag or solar pressure. The following equation (since exhaust velocity is negative) relates the velocity of the exhaust V_e in the observer frame to the exhaust velocity in the rocket frame v_e:

$$V_e = V - v_e$$

Given $dm = -\Delta m$ (since ejecting a positive Δm results in a mass drop) and $\sum F_i = 0$ (i.e. no external forces), the (4.1) yields:

$$\Delta V = v_e \ln \frac{m_0}{m_1} \tag{4.2}$$

where:

- ΔV (delta-v) is the greatest velocity change of the vehicle;

- m_0 is the starting mass, which includes the propellant;

- m_f is the ultimate overall mass excluding the propellant;

- The effective exhaust velocity is denoted by v_e.

The following equation connects the parameter v_e to the thruster specific impulse I_{sp} and the standard gravity g_0:

$$v_e = I_{sp}g_0$$

The Tsiolkovsky rocket equation was developed by assuming that the body whose motion is being studied is solely subject to the action of the motor's push; it does not account for the effect of gravitational or aerodynamic forces. So it would be precise only for describing the rocket velocity in a vacuum. However, it may be used efficiently in orbital manoeuvres to estimate how much propellant is required to shift to a certain new orbit or to locate the new orbit as a result of a specific propellant burn.

4.3.2   In-space propulsion description

In-space is defined as the zone beyond Earth's gravitational pull till the Geostationary Earth Orbit (GEO) at 35.786 km above the Earth's surface. Strategic communications assets, rapid warning, Earth observation, navigation, reconnaissance, surveillance, and weather are all examples of Earth monitoring systems that are housed in this region. Then, because we're talking about LEO-GEO orbit manoeuvres, in-space thrusters are taken into account in the investigation of the propulsion systems employed for the autonomous mission. Their key duties are, in general, primary propulsion, reaction control, station holding, precision pointing, and orbital manoeuvring. They are divided into three major groups.

1. Chemical: solid, liquid and hybrid

2. Cold gas

3. Electric

Chemical propulsion

Chemical thrusters are endothermic actuators because they do not require external power, but instead use the internal energy of the propellant through combustion and chemical processes. Because their ejection velocity is restricted by the combustion/reaction temperature, they can deliver extremely high thrust, as in launch vehicles, at the price of a huge expelled mass. They are utilised for sudden and quick movements because to their major characteristics of strong thrust capacity, high levels of specific impulse, and short ON mode duration.
Below are reported the main chemical propulsion systems, as listed in [16]:

- SOLID FUEL PROPULSION: All of the components necessary for strong combustion are combined together and packed into a solid cylinder, as illustrated in Figure 4.2, to form a single material in a solid rocket fuel grain. When the combustion begins, it continues until the propellant is depleted. An oxidizer, a fuel or other solid hydrocarbon, and an accelerant will be present. When ignited, the fuel grain will burn rapidly, generating a significant volume of hot gases that will create thrust.
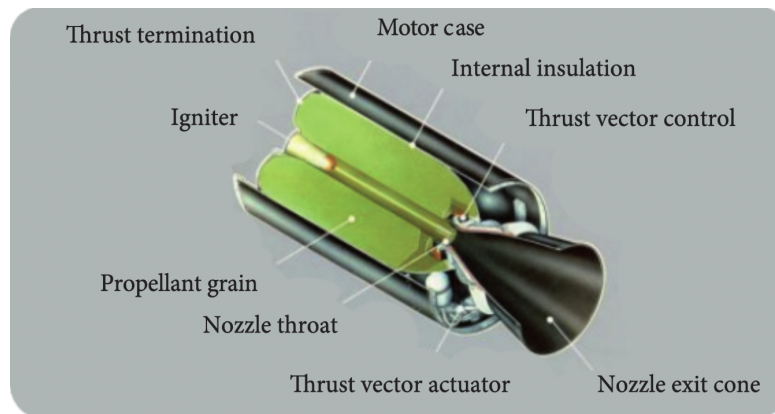
Figure 4.2: Solid chemical propulsion system

- LIQUID FUEL PROPULSION: the propellant is made up of two composites: fuel and oxidizer. They are held separately in liquid tanks before being pushed into the nozzle combustion chamber, where they burn. By cutting off the propellant flow, the engine may cease the combustion and thrust. Because of the pumps and storage tanks, liquid rockets are heavier and more sophisticated.

- HYBRID PROPULSION: It is a rocket with an engine that employs rocket propellants in two states: solid and either gas or liquid. It is made up of a pressure vessel (tank) that contains the liquid oxidiser, a combustion chamber

that contains the solid propellant, and a mechanism that separates the two. When thrust is required, the valve is opened and an appropriate ignition source is supplied into the combustion chamber. The liquid propellant (or gas) enters the combustion chamber and is evaporated before reacting with the solid propellant. Combustion takes place in a boundary layer diffusion flame at the surface of the solid propellant.

Cold gas propulsion

A cold gas thruster is a type of propeller that employs pressured inert gas as the reaction mass. To create a cold jet thrust, the compressed gas is expelled via a propelling nozzle. This thruster typically comprises of a pressurised tank storing gas, a valve to regulate its release, a propelling nozzle, and tubing connecting them, as shown in Figure 4.3. Because the gas is generally unheated, the speed at the throat is low, and the performance is quite low. As a result, cold gas propulsion is employed for the following purposes:

- Extremely precise attitude control;

- Solar radiation pressure and other environmental disturbances are accounted for;

- Drag-free control in real time;

- Formation flying maintenance and mutual position control.
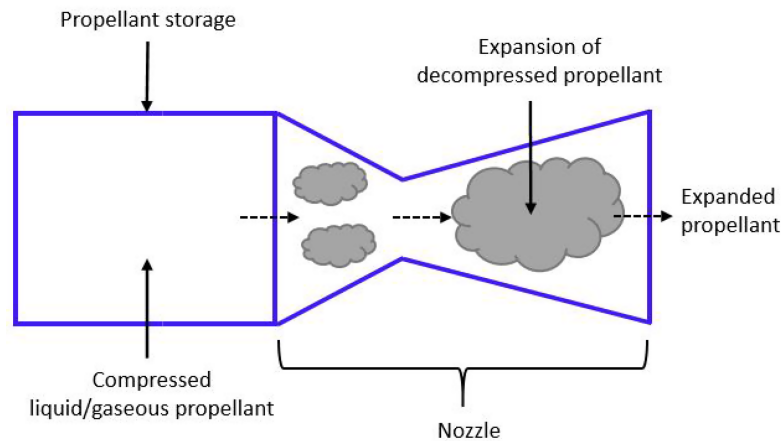
Figure 4.3: Cold gas propulsion system

49

Electric propulsion

According to [17], electric propulsion is a technique that aims to achieve thrust with high exhaust velocities, resulting in a lower quantity of propellant required for a particular space mission or application as compared to other traditional propulsion systems. Reduced propellant mass can drastically reduce a spacecraft or satellite's launch mass, resulting in cheaper costs due to the utilisation of smaller launch vehicles to deliver a desired mass into a specific orbit or to a deep-space destination.

Electric thrusters are typically defined by the acceleration mechanism utilised to generate thrust. These techniques are simply classified into three types: electrothermal, electrostatic, and electromagnetic.

Electrothermal thrusters

The electrothermal category includes devices that produce plasma using electromagnetic fields to raise the temperature of the bulk propellant. A nozzle converts the thermal energy supplied to the propellant gas into kinetic energy. Gases of low molecular weight are employed (e.g. hydrogen, helium, ammonia). Here are several examples:

1. **Resistojet**

   Resistojets are electrothermal devices in which the propellant is heated before entering a downstream nozzle by passing through a resistively heated chamber or over a resistively heated element. The rise in exhaust velocity is caused by the propellant thermal heating, which restricts the I_{sp} to low values (<500 s).

2. **Arcjet**

   An arcjet is another type of electrothermal thruster that warms the propellant by passing it via a high current arc connected to the nozzle feed system. While there is an electric discharge in the propellant passage, plasma effects in the exhaust velocity are minor since the propellant is weakly ionised. Thermal heating limits the I_{sp} to less than 700 s for easily stored propellants.

Electrostatic thrusters

The acceleration is caused by Coulomb force, which is the use of a static electric field in the same direction of the acceleration. Here are a few examples:

1. **Ion Thruster**

   To ionise a considerable portion of the fuel, ion thrusters use a multitude of plasma generating mechanisms. These thrusters then use biassed grids to electrostatically collect ions from the plasma and accelerate them to high velocity at voltages exceeding 10 kV. When compared to other thruster types, ion thrusters have the highest efficiency (from 60% to >80%) and the largest specific impulse (from 2000 to over 10,000 s).

2. **Hall Thruster**

   To create plasma, this type of electrostatic thruster employs a cross-field discharge defined by the Hall effect. An electric field perpendicular to an applied magnetic field electrostatically accelerates ions to high exhaust velocities, whilst the transverse magnetic field suppresses electron mobility that would otherwise short out the electric field. The efficiency and specific impulse of Hall thrusters are somewhat lower than those of ion thrusters, but the thrust at a given power is greater, and the device is more simpler and requires less power supply to work.

Electromagnetic thrusters

Electromagnetic thrusters accelerate ions using either the Lorentz force or the influence of electromagnetic fields in which the electric field is not pointing in the direction of acceleration. Here are several examples:

1. **Pulsed Plasma Thruster**

   A pulsed plasma thruster (PPT) is an electromagnetic thruster that uses a pulsed discharge to ionise a fraction of a solid propellant ablated into a plasma arc, followed by electromagnetic effects in the pulse to accelerate the ions to high exit velocity. The thrust level is determined by the rate of pulse repetition.

2. **Magnetoplasmadynamic Thruster**

   Magnetoplasmadynamic (MPD) thrusters are electromagnetic devices that employ a high-current arc to ionise a major portion of the propellant and then

51

use electromagnetic forces (Lorentz $\mathbf{J} \times \mathbf{B}$ forces) in the plasma discharge to accelerate the charged propellant. Because plasma discharges often create both current and magnetic fields, MPD thrusters tend to run at extremely high powers in order to generate adequate force for high specific impulse operation, and so generate high thrust when compared to the other technologies discussed above.
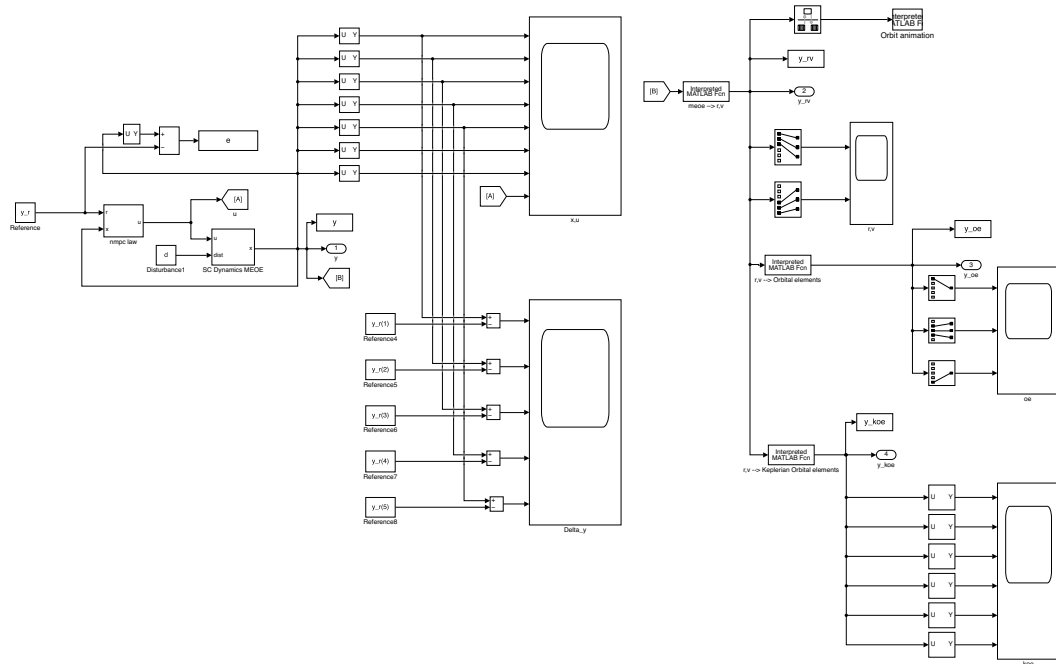
Chapter 5

Simulation and results

In this chapter will be reported the simulation environment developed in MAT-LAB/Simulink, analyzing main blocks, and the results obtained.

5.1 Simulation environment

To simulate the space mission behaviour, Simulink schemes jointly with MATLAB scripts have been used, as reported in Figure 5.1.

Figure 5.1: Simulink simulation environment

53

The main blocks are:

- Reference: in this block the target orbit is defined in MEOE coordinates;

- SC Dynamics MEOE: in this block the S/C dynamics expressed in MEOE coordinates is obtained;

- NMPC law: in this block the Pontryagin-based NMPC algorithm is implemented.

An accurate explanation of each block is provided here to give a thorough knowledge of how the simulation environment was created.

5.1.1 Reference block

As reported in Section 2.9, here is defined the target GEO orbit that is circular ($e = 0$) and equatorial ($i = 0$), with a semi-major axis $a = 42164 \ km$. Below the reference vector:

$$\boldsymbol{y}_r = \begin{bmatrix} p_r \\ f_r \\ g_r \\ h_r \\ k_r \end{bmatrix} = \begin{bmatrix} 42164 \\ 0 \\ 0 \\ 0 \\ 0 \end{bmatrix} \tag{5.1}$$

As can be noticed, the final dimension of the reference vector is equal to five, because the true longitude parameter L has been left free since we are not interested in the exact position along the orbit.

5.1.2 S/C Dynamics MEOE block

A model for modelling S/C behaviour may be defined as a mathematical description of the physical attributes of the system; in general, this is a state space representation, i.e. a collection of first order differential equations of the form:

$$\dot{\mathbf{x}}(t) = f[\mathbf{x}(t), \mathbf{u}(t); t]$$
$$\mathbf{y}(t) = h[\mathbf{x}(t), \mathbf{u}(t); t]$$

Before moving to describe the S/C dynamics, it is necessary to report the initial state conditions. As described in Section 2.9, the initial LEO orbit is circular ($e = 0$) and equatorial ($i = 0$), with a semi-major axis $a = 6771 \ km$. Moreover, since we have to take into account also the mass variation, according to the Tsiolkovsky rocket equation, the initial state vector $\boldsymbol{x}_0$ will not be a 6-dimensional vector but a 7-dimensional one, where the last term is m_0, i.e. the initial total mass given by the

S/C mass plus the fuel mass. Below this vector is reported for sake of completeness:

$$\boldsymbol{x}_0 = \begin{bmatrix} p_0 \\ f_0 \\ g_0 \\ h_0 \\ k_0 \\ m_0 \end{bmatrix} = \begin{bmatrix} 6771 \\ 0 \\ 0 \\ 0 \\ 0 \\ 5000 \end{bmatrix} \tag{5.2}$$

In particular, Modified equinoctial orbital elements dynamics and Tsiolkovsky rocket equation, respectively described in Subsection 2.8.4 and Subsection 4.3.1, has been used to describe completely the S/C dynamics, as reported below:

$$\dot{p} = \frac{dp}{dt} = \frac{2p}{w}\sqrt{\frac{p}{\mu}}\Delta_t$$

$$\dot{f} = \frac{df}{dt} = \sqrt{\frac{p}{\mu}}\left[\Delta_r \sin L + [(w+1)\cos L + f]\frac{\Delta_t}{w} - (h\sin L - k\cos L)\frac{g\Delta_n}{w}\right]$$

$$\dot{g} = \frac{dg}{dt} = \sqrt{\frac{p}{\mu}}\left[-\Delta_r \cos L + [(w+1)\sin L + g]\frac{\Delta_t}{w} + (h\sin L - k\cos L)\frac{g\Delta_n}{w}\right]$$

$$\dot{h} = \frac{dh}{dt} = \sqrt{\frac{p}{\mu}}\frac{s^2\Delta_n}{2w}\cos L$$

$$\dot{k} = \frac{dk}{dt} = \sqrt{\frac{p}{\mu}}\frac{s^2\Delta_n}{2w}\sin L$$

$$\dot{L} = \frac{dL}{dt} = \sqrt{\mu p}\left(\frac{w}{p}\right)^2 + \frac{1}{w}\sqrt{\frac{p}{\mu}}(h\sin L - k\cos L)\Delta_n$$

$$\dot{m} = \frac{dm}{dt} = \frac{\|T\|_q}{I_{sp}g_0} = \frac{-1000m\|u\|_2}{I_{sp}g_0}, \quad u = \Delta_r\hat{\mathbf{i}}_r + \Delta_t\hat{\mathbf{i}}_t + \Delta_n\hat{\mathbf{i}}_n$$

$$\tag{5.3}$$

that in state space representation becomes:

$$\dot{x}_1 = \frac{2x_1}{w}\sqrt{\frac{x_1}{\mu}}u_2$$

$$\dot{x}_2 = \sqrt{\frac{x_1}{\mu}}\left[u_1\sin x_6 + [(w+1)\cos x_6 + x_2]\frac{u_2}{w} - (x_4\sin x_6 - x_5\cos x_6)\frac{x_3 u_3}{w}\right]$$

$$\dot{x}_3 = \sqrt{\frac{x_1}{\mu}}\left[-u_1\cos x_6 + [(w+1)\sin x_6 + x_3]\frac{u_2}{w} + (x_4\sin x_6 - x_5\cos x_6)\frac{x_3 u_3}{w}\right]$$

$$\dot{x}_4 = \sqrt{\frac{x_1}{\mu}}\frac{s^2 u_3}{2w}\cos x_6$$

$$\dot{x}_5 = \sqrt{\frac{x_1}{\mu}}\frac{s^2 u_3}{2w}\sin x_6$$

$$\dot{x}_6 = \sqrt{\mu x_1}\left(\frac{w}{x_1}\right)^2 + \frac{1}{w}\sqrt{\frac{x_1}{\mu}}(x_4\sin x_6 - x_5\cos x_6)u_3$$

$$\dot{x}_7 = \frac{-1000x_7\|u\|_2}{I_{sp}g_0}$$

(5.4)

where $w = 1 + x_2\cos x_6 + x_3\sin x_6$ and $s^2 = 1 + x_4^2 + x_5^2$. Parameters $I_{sp} = 3{,}000\,\text{s}$ (typical of electric propulsion systems), $g_0 = 9.807\,\text{m/s}^2$ and $\mu = 398{,}600.44\,\text{km}^3/\text{s}^2$ that is the *Gravitational parameter*. At the end, modified equinoctial orbital elements and mass values at each instant of time were determined using numerical integration.

The output vector of the plant y will be a five dimensional vector, as reported in the following:

$$\boldsymbol{y} = \begin{bmatrix} x_1 \\ x_2 \\ x_3 \\ x_4 \\ x_5 \end{bmatrix} = \begin{bmatrix} p \\ f \\ g \\ h \\ k \end{bmatrix}$$

(5.5)

This choice is mainly due to the fact that we are not interested, as reported in previous chapters, to control the exact position of the S/C along the orbit, that means we can keep free $x_6 = L$. Moreover, in order to control the mass variable $x_7 = m$, further models must be used to find its boundary conditions, so, in this thesis, it has not been taken into as control variable. These choices allow to relax, computationally speaking, the control algorithm.

5.1.3 NMPC law

A simplified model, as explained before, is needed for the prediction phase in order to solve the optimization problem. In formulae:

$$\dot{\hat{x}}_1 = \frac{2\hat{x}_1}{\hat{w}}\sqrt{\frac{\hat{x}_1}{\mu}}u_2$$

$$\dot{\hat{x}}_2 = \sqrt{\frac{\hat{x}_1}{\mu}}\left[u_1\sin\hat{x}_6 + [(\hat{w}+1)\cos\hat{x}_6 + \hat{x}_2]\frac{u_2}{\hat{w}} - (\hat{x}_4\sin\hat{x}_6 - \hat{x}_5\cos\hat{x}_6)\frac{\hat{x}_3 u_3}{\hat{w}}\right]$$

$$\dot{\hat{x}}_3 = \sqrt{\frac{\hat{x}_1}{\mu}}\left[-u_1\cos\hat{x}_6 + [(\hat{w}+1)\sin\hat{x}_6 + \hat{x}_3]\frac{u_2}{\hat{w}} + (\hat{x}_4\sin\hat{x}_6 - \hat{x}_5\cos\hat{x}_6)\frac{\hat{x}_3 u_3}{\hat{w}}\right]$$

$$\dot{\hat{x}}_4 = \sqrt{\frac{\hat{x}_1}{\mu}}\frac{\hat{s}^2 u_3}{2\hat{w}}\cos\hat{x}_6$$

$$\dot{\hat{x}}_5 = \sqrt{\frac{\hat{x}_1}{\mu}}\frac{\hat{s}^2 u_3}{2\hat{w}}\sin\hat{x}_6$$

$$\dot{\hat{x}}_6 = \sqrt{\mu\hat{x}_1}\left(\frac{\hat{w}}{\hat{x}_1}\right)^2 + \frac{1}{\hat{w}}\sqrt{\frac{\hat{x}_1}{\mu}}(\hat{x}_4\sin\hat{x}_6 - \hat{x}_5\cos\hat{x}_6)u_3$$

$$\dot{\hat{x}}_7 = 0$$

$$(5.6)$$

In this way, it is possible to define the *predicted tracking error* as the difference between the reference signal and the prediction output, that is:

$$\tilde{\boldsymbol{y}} = \boldsymbol{y}_r - \hat{\boldsymbol{y}} \tag{5.7}$$

where $\hat{\boldsymbol{y}} = \begin{bmatrix} \hat{x}_1 & \hat{x}_2 & \hat{x}_3 & \hat{x}_4 & \hat{x}_5 \end{bmatrix}^T$.

To solve the dual optimization problem, i.e. a TBVP, it is convenient to define a new augmented state vector $\boldsymbol{\xi} = \begin{bmatrix} \boldsymbol{x} & \boldsymbol{\lambda} \end{bmatrix}^T$ that includes the S/C state variables to be controlled and their corresponding co-states variables. Its dynamics $\dot{\boldsymbol{\xi}}$ is equal to:

$$\dot{\boldsymbol{\xi}} = \begin{bmatrix} \dot{\boldsymbol{x}}_1 \\ \vdots \\ \dot{\boldsymbol{x}}_5 \\ \dot{\boldsymbol{\lambda}}_1 \\ \vdots \\ \dot{\boldsymbol{\lambda}}_5 \end{bmatrix} \tag{5.8}$$

57

whose first five elements are obtained from (5.4) and the others five by solving (3.4). The explicit form is shown below:

$$\dot{\xi}_1 = \frac{2\,\xi_1}{w}\sqrt{\frac{\xi_1}{\mu}}\,u_2^*$$

$$\dot{\xi}_2 = \sqrt{\frac{\xi_1}{\mu}}\left[u_1^*\,\sin\left(\delta\right) + \left[(w+1)\,\cos\left(\delta\right) + \xi_2\right]\frac{u_2^*}{w} - \left(\xi_4\,\sin\left(\delta\right) - \xi_5\,\cos\left(\delta\right)\right)\frac{\xi_3\,u_3^*}{w}\right]$$

$$\dot{\xi}_3 = \sqrt{\frac{\xi_1}{\mu}}\left[-u_1^*\,\cos\left(\delta\right) + \left[(w+1)\,\sin\left(\delta\right) + \xi_3\right]\frac{u_2^*}{w} + \left(\xi_4\,\sin\left(\delta\right) - \xi_5\,\cos\left(\delta\right)\right)\frac{\xi_3\,u_3^*}{w}\right]$$

$$\dot{\xi}_4 = \sqrt{\frac{\xi_1}{\mu}}\frac{s^2\,u_3^*}{2\,w}\,\cos\left(\delta\right)$$

$$\dot{\xi}_5 = \sqrt{\frac{\xi_1}{\mu}}\frac{s^2\,u_3^*}{2\,w}\,\sin\left(\delta\right)$$

$$\dot{\xi}_6 = -\frac{1}{4\,\mu\,\sqrt{\frac{\xi_1}{\mu}}\,\left(\xi_2\,\cos\left(\delta\right) + \xi_3\,\sin\left(\delta\right) + 1\right)}\Big[4\,\xi_7\,u_2^*\,\cos\left(\delta\right) - 2\,\xi_8\,u_1^*\,\cos\left(\delta\right) +$$

$$+ \xi_9\,u_3^*\,\cos\left(\delta\right) + 2\,\xi_7\,u_1^*\,\sin\left(\delta\right) + 4\,\xi_8\,u_2^*\,\sin\left(\delta\right) + \xi_{10}\,u_3^*\,\sin\left(\delta\right) + 12\,\xi_6\,u_2^*\,\xi_1 +$$

$$+ 2\,\xi_7\,u_2^*\,\xi_2 + 2\,\xi_8\,u_2^*\,\xi_3 + \xi_7\,u_1^*\,\xi_2\,\sin\left(2\,\delta\right) + \xi_7\,u_2^*\,\xi_3\,\sin\left(2\,\delta\right) - \xi_8\,u_1^*\,\xi_3\,\sin\left(2\,\delta\right) +$$

$$+ \xi_8\,u_2^*\,\xi_2\,\sin\left(2\,\delta\right) + 2\,\xi_7\,u_1^*\,\xi_3\,\sin\left(\delta\right)^2 + 2\,\xi_8\,u_2^*\,\xi_3\,\sin\left(\delta\right)^2 + \xi_{10}\,u_3^*\,\xi_4^{\,2}\,\sin\left(\delta\right) +$$

$$+ \xi_{10}\,u_3^*\,\xi_5^{\,2}\,\sin\left(\delta\right) + 2\,\xi_7\,u_2^*\,\xi_2\,\cos\left(\delta\right)^2 - 2\,\xi_8\,u_1^*\,\xi_2\,\cos\left(\delta\right)^2 + \xi_9\,u_3^*\,\xi_4^{\,2}\,\cos\left(\delta\right) +$$

$$+ \xi_9\,u_3^*\,\xi_5^{\,2}\,\cos\left(\delta\right) + 2\,\xi_7\,u_3^*\,\xi_3\,\xi_5\,\cos\left(\delta\right) - 2\,\xi_8\,u_3^*\,\xi_3\,\xi_5\,\cos\left(\delta\right) +$$

$$- 2\,\xi_7\,u_3^*\,\xi_3\,\xi_4\,\sin\left(\delta\right) + 2\,\xi_8\,u_3^*\,\xi_3\,\xi_4\,\sin\left(\delta\right)\Big] - 2\,Q_{1,1}\,(\xi_1 - y_{r,1})$$

$$\dot{\xi}_7 = \frac{\sqrt{\frac{\xi_1}{\mu}}}{2\,\left(\xi_2\,\cos\left(\delta\right) + \xi_3\,\sin\left(\delta\right) + 1\right)^2}\Big[2\,\xi_7\,u_2^*\,\cos\left(\delta\right)^2 - 2\,\xi_7\,u_2^* +$$

$$+ \xi_9\,u_3^*\,\cos\left(\delta\right)^2 + \xi_8\,u_2^*\,\sin\left(2\,\delta\right) + \frac{\xi_{10}\,u_3^*\,\sin\left(2\,\delta\right)}{2} + \xi_9\,u_3^*\,\xi_4^{\,2}\,\cos\left(\delta\right)^2 +$$

$$+ \xi_9\,u_3^*\,\xi_5^{\,2}\,\cos\left(\delta\right)^2 + \frac{\xi_{10}\,u_3^*\,\xi_4^{\,2}\,\sin\left(2\,\delta\right)}{2} + \frac{\xi_{10}\,u_3^*\,\xi_5^{\,2}\,\sin\left(2\,\delta\right)}{2} + 4\,\xi_6\,u_2^*\,\xi_1\,\cos\left(\delta\right) +$$

$$+ 2\,\xi_8\,u_2^*\,\xi_3\,\cos\left(\delta\right) - 2\,\xi_7\,u_2^*\,\xi_3\,\sin\left(\delta\right) + 2\,\xi_7\,u_3^*\,\xi_3\,\xi_5\,\cos\left(\delta\right)^2 +$$

$$- 2\,\xi_8\,u_3^*\,\xi_3\,\xi_5\,\cos\left(\delta\right)^2 - \xi_7\,u_3^*\,\xi_3\,\xi_4\,\sin\left(2\,\delta\right) + \xi_8\,u_3^*\,\xi_3\,\xi_4\,\sin\left(2\,\delta\right)\Big] +$$

$$- 2\,Q_{2,2}\,(\xi_2 - y_{r,2})$$

$$\dot{\xi}_8 = \frac{\sqrt{\frac{\xi_1}{\mu}}}{2\left(\xi_2\,\cos\left(\delta\right)+\xi_3\,\sin\left(\delta\right)+1\right)^2}\left[\xi_7\,u_2^*\,\sin\left(2\,\delta\right)-2\,\xi_8\,u_2^*+\frac{\xi_9\,u_3^*\,\sin\left(2\,\delta\right)}{2}+\right.$$
$$+2\,\xi_8\,u_2^*\sin\left(\delta\right)^2+\xi_{10}\,u_3^*\sin\left(\delta\right)^2+\frac{\xi_9\,u_3^*\,\xi_4^2\,\sin\left(2\,\delta\right)}{2}+\frac{\xi_9\,u_3^*\,\xi_5^2\,\sin\left(2\,\delta\right)}{2}+$$
$$+\xi_{10}\,u_3^*\,\xi_4^2\sin\left(\delta\right)^2+\xi_{10}\,u_3^*\,\xi_5^2\sin\left(\delta\right)^2-2\,\xi_8\,u_2^*\,\xi_2\,\cos\left(\delta\right)-2\,\xi_7\,u_3^*\,\xi_5\,\cos\left(\delta\right)+$$
$$+2\,\xi_8\,u_3^*\,\xi_5\,\cos\left(\delta\right)+4\,\xi_6\,u_2^*\,\xi_1\,\sin\left(\delta\right)+2\,\xi_7\,u_2^*\,\xi_2\,\sin\left(\delta\right)+2\,\xi_7\,u_3^*\,\xi_4\,\sin\left(\delta\right)+$$
$$-2\,\xi_8\,u_3^*\,\xi_4\,\sin\left(\delta\right)-2\,\xi_7\,u_3^*\,\xi_2\,\xi_5\,\cos\left(\delta\right)^2+2\,\xi_8\,u_3^*\,\xi_2\,\xi_5\,\cos\left(\delta\right)^2+$$
$$\left.+\xi_7\,u_3^*\,\xi_2\,\xi_4\,\sin\left(2\,\delta\right)-\xi_8\,u_3^*\,\xi_2\,\xi_4\,\sin\left(2\,\delta\right)\right]-2\,Q_{3,3}\left(\xi_3-y_{r,3}\right)$$
$$\dot{\xi}_9 = -\frac{u_3^*\,\sqrt{\frac{\xi_1}{\mu}}\,\left(\xi_9\,\xi_4\,\cos\left(\delta\right)-\xi_7\,\xi_3\,\sin\left(\delta\right)+\xi_8\,\xi_3\,\sin\left(\delta\right)+\xi_{10}\,\xi_4\,\sin\left(\delta\right)\right)}{\xi_2\,\cos\left(\delta\right)+\xi_3\,\sin\left(\delta\right)+1}+$$
$$-2\,Q_{4,4}\left(\xi_4-y_{r,4}\right)$$
$$\dot{\xi}_{10} = -\frac{u_3^*\,\sqrt{\frac{\xi_1}{\mu}}\,\left(\xi_7\,\xi_3\,\cos\left(\delta\right)-\xi_8\,\xi_3\,\cos\left(\delta\right)+\xi_9\,\xi_5\,\cos\left(\delta\right)+\xi_{10}\,\xi_5\,\sin\left(\delta\right)\right)}{\xi_2\,\cos\left(\delta\right)+\xi_3\,\sin\left(\delta\right)+1}+$$
$$-2\,Q_{5,5}\left(\xi_5-y_{r,5}\right)$$

$$(5.9)$$

where $w = 1 + \xi_2\,\cos\left(\delta\right)+\xi_3\sin\left(\delta\right)$ and $s^2 = 1 + \xi_4^2 + \xi_5^2$, $\delta = \hat{L} = \hat{x}_6$ acting as external disturbance to the augmented plant. Regarding the augmented state initial conditions, they are given by:

$$\dot{\boldsymbol{\xi}}_0 = \left[\begin{array}{c} \boldsymbol{x}_0 \\ \boldsymbol{\lambda}_0 \end{array}\right]$$

$$(5.10)$$

where $\boldsymbol{\lambda}_0 = O_{5\times1}$.

For what concerning the optimal control input u^*, it has been obtained solving (3.8). The analytical equation, related to the three components, i.e. radial, tangential and normal respectively, is reported below:

$$u_1^* = -\frac{1}{2\,R_{1,1}} \left[\sqrt{\frac{\xi_1}{\mu}} \, (\xi_7\,\sin{(\delta)} - \xi_8\,\cos{(\delta)}) \right]$$

$$u_2^* = -\frac{1}{2\,R_{2,2}} \frac{\sqrt{\frac{\xi_1}{\mu}}}{\xi_2\,\cos{(\delta)} + \xi_3\,\sin{(\delta)} + 1} \left[\xi_7\,\xi_2\cos{(\delta)}^2 + 2\,\xi_7\,\cos{(\delta)} + \right.$$

$$+ \xi_8\,\xi_3\sin{(\delta)}^2 + 2\,\xi_8\,\sin{(\delta)} + 2\,\xi_6\,\xi_1 + \xi_7\,\xi_2 + \xi_8\,\xi_3 + \frac{\xi_7\,\xi_3\,\sin{(2\,\delta)}}{2} +$$

$$\left. + \frac{\xi_8\,\xi_2\,\sin{(2\,\delta)}}{2} \right]$$

$$u_3^* = -\frac{1}{2\,R_{3,3}} \frac{\sqrt{\frac{\xi_1}{\mu}}}{2\,(\xi_2\,\cos{(\delta)} + \xi_3\,\sin{(\delta)} + 1)} \left[\xi_9\,\cos{(\delta)} + \right.$$

$$+ \xi_{10}\,\sin{(\delta)} + \xi_9\,\xi_4{}^2\,\cos{(\delta)} + \xi_9\,\xi_5{}^2\,\cos{(\delta)} + \xi_{10}\,\xi_4{}^2\,\sin{(\delta)} + \xi_{10}\,\xi_5{}^2\,\sin{(\delta)} +$$

$$\left. + 2\,\xi_7\,\xi_3\,\xi_5\,\cos{(\delta)} - 2\,\xi_8\,\xi_3\,\xi_5\,\cos{(\delta)} - 2\,\xi_7\,\xi_3\,\xi_4\,\sin{(\delta)} + 2\,\xi_8\,\xi_3\,\xi_4\,\sin{(\delta)} \right]$$

$$(5.11)$$

In order to obtain the best trade-off between requirements and performances, several simulation campaigns have been performed. The tuning process, concerning the parameters reported in Subsection 3.9.1, has been done by trial and error procedure. The following table resumes the chosen values:

NMPC Parameters	
P weight matrix	$\begin{bmatrix} 15 & 0 & 0 & 0 & 0 \\ 0 & 1\times10^{12} & 0 & 0 & 0 \\ 0 & 0 & 1\times10^9 & 0 & 0 \\ 0 & 0 & 0 & 5\times10^1 & 0 \\ 0 & 0 & 0 & 0 & 5\times10^1 \end{bmatrix}$
Q weight matrix	$\begin{bmatrix} 1 & 0 & 0 & 0 & 0 \\ 0 & 1\times10^6 & 0 & 0 & 0 \\ 0 & 0 & 1\times10^8 & 0 & 0 \\ 0 & 0 & 0 & 1 & 0 \\ 0 & 0 & 0 & 0 & 1 \end{bmatrix}$
R weight matrix	$\begin{bmatrix} 1\times10^{15} & 0 & 0 \\ 0 & 1\times10^{17} & 0 \\ 0 & 0 & 1\times10^{15} \end{bmatrix}$
Sampling time $\mathbf{T}_s$	3600 s
Prediction horizon $\mathbf{T}_p$	10800 s
Control horizon $\mathbf{T}_c$	10800 s
Input upper bound $\mathbf{u}_{MAX}$	$+F_{MAX}/m_0 = 0.02$ m/s^2
Input lower bound $\mathbf{u}_{MIN}$	$-F_{MAX}/m_0 = -0.02$ m/s^2

Table 5.1: NMPC design parameters

As can be noticed by the table, in matrices **P** and **Q** the second and the third elements on the diagonal have higher values with respect to the other, since the second and third elements of state vector, i.e. f and g respectively, require more weight cause their transient is longer with respect to the other state variables. The maximum force $\mathbf{F}_{MAX}$ that the actuators can provide has been chosen equal to 100 N.

5.2   Plots

The simulation was carried out for a simulation time $T_{sim} = 2592000$ s ≈ 1 month and with a zero disturbance vector entering the S/C Dynamics MEOE block, that means without taking into account non-spherical gravitational acceleration, aerodynamic drag and secondary body perturbations effects. In the following are reported the most significant variable plots
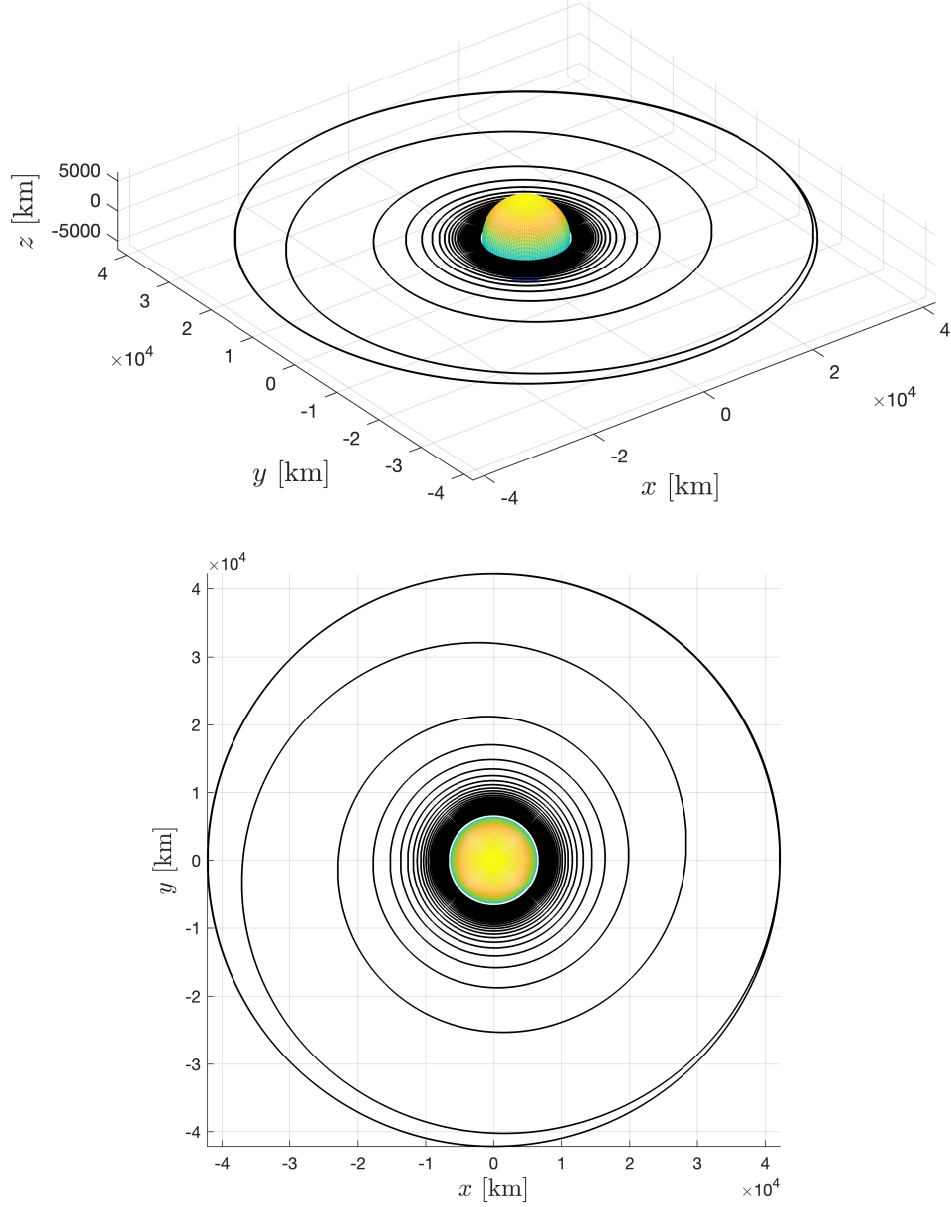

Figure 5.2: S/C orbit

State & Control Input
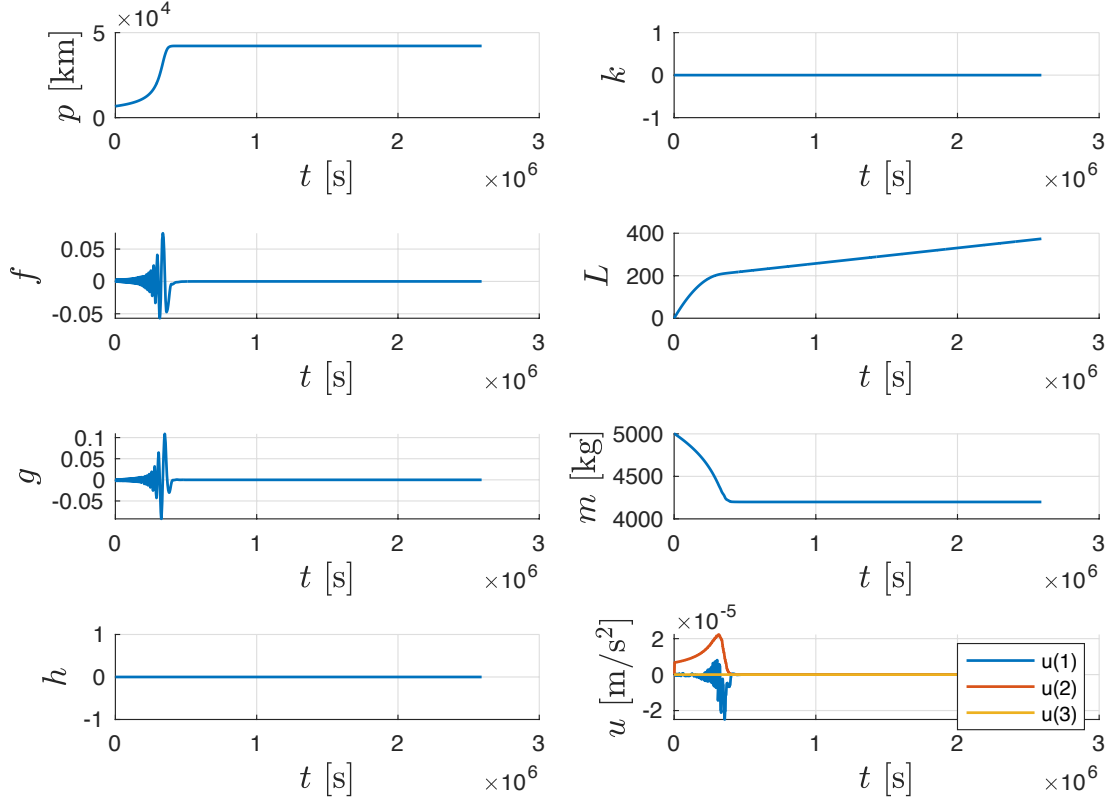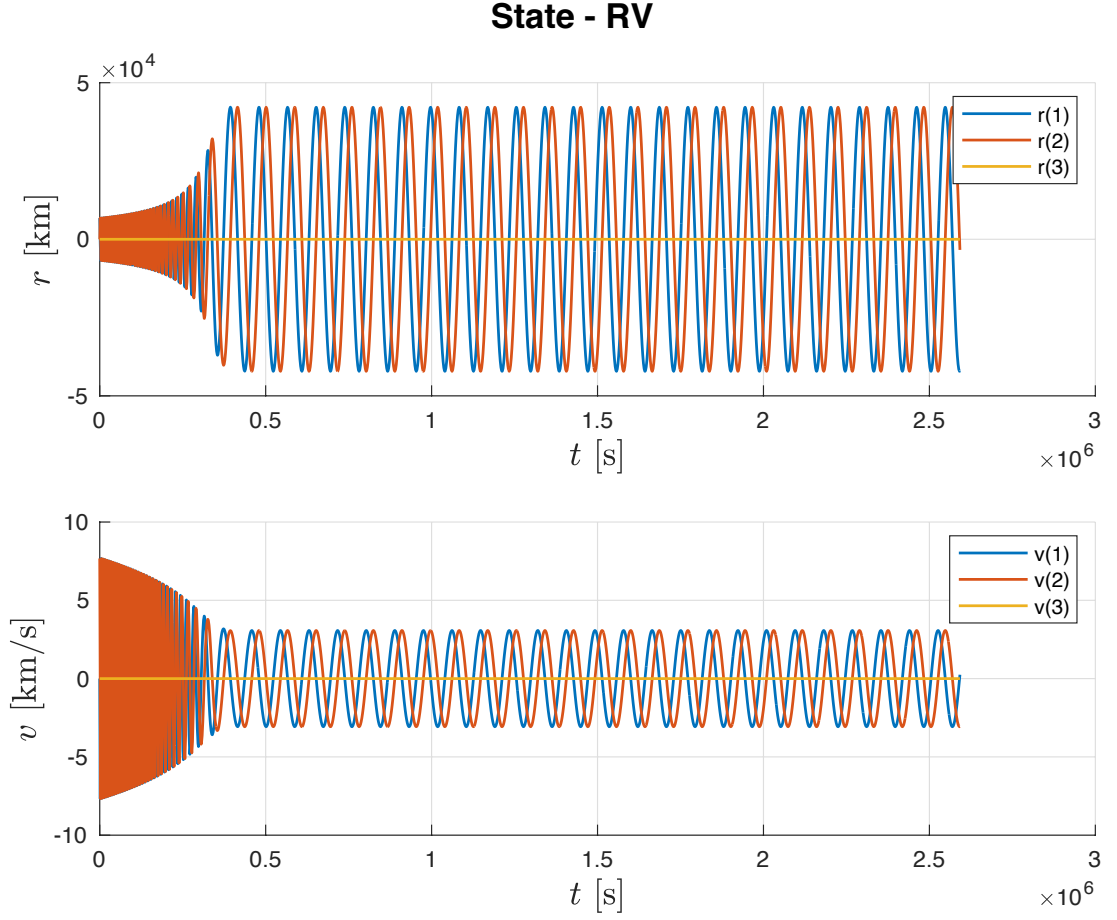

Figure 5.3: State variables expressed in MEOE and control input

The final orbit is reached after $t = 6 \times 10^5$ s ≈ 7 days, due to the higher transient of f and g. The mass variation in percentage is equal to 16.02 %, that means a propellant consumption of 801.1 kg. This result is reasonable according to the actual literature. It is also interesting to notice that the third control input component, i.e. the normal one, is always zero cause the mission is coplanar ($i = 0$).

State - KOE
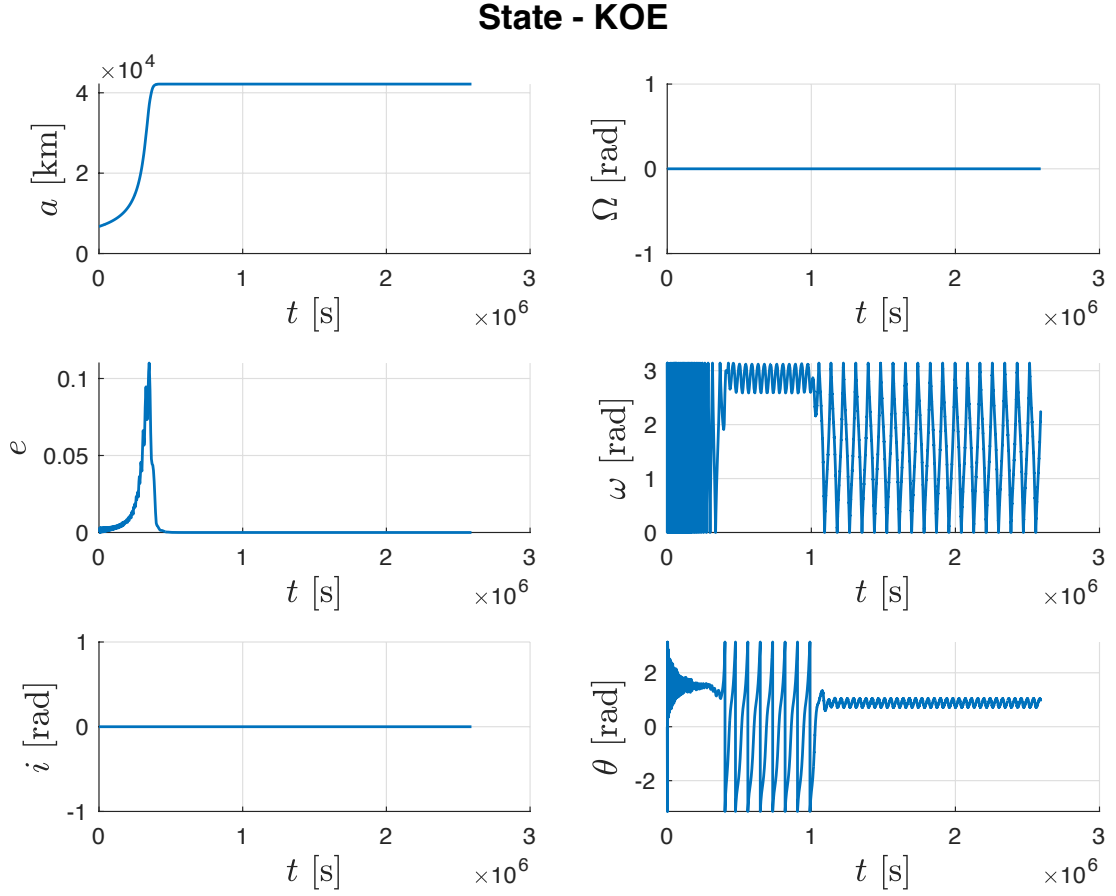
Figure 5.4: State variables expressed in KOE

As reported in Subsection 2.7.1 and Section 2.8, the Keplerian Orbital Elements have singularities for zero eccentricity and zero orbital inclination; this can be noticed by the behaviour of ω and θ.

State - RV

Figure 5.5: State variables expressed in RV

A further proof of the mission fulfillment is given by the RV state variable representation. In particular, the position vector r shows that the final orbit is perfectly circular ($e = 0$) and coplanar ($i = 0$) since the first two components, i.e. the radial and tangential ones, assume values 42164 km (target semilatus rectum) and the third one is always zero, as explaine before.

65
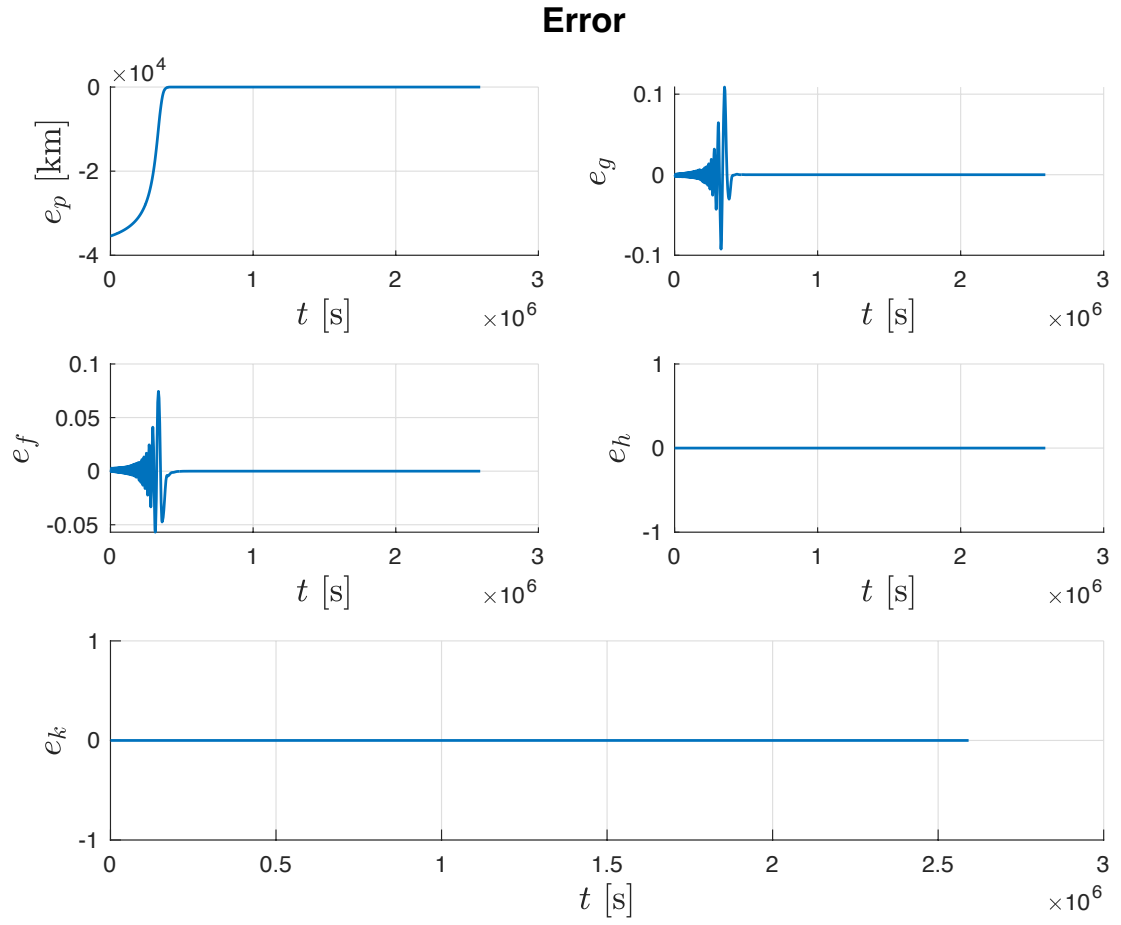
Error

Figure 5.6: Tracking error

Chapter 6

Conclusions

In this thesis, a constrained NMPC control algorithm based on Pontryagin Minimum Principle approach has been developed for space missions. In particular, the goal has been to transfer a S/C from a circular and equatorial Low Earth Orbit to a circular and equatorial Geostationary Orbit, adopting a low-thrust strategy.

First of all, a S/C dynamics based on the Modified Equinoctial Orbital Elements has been adopted. These equations allow us to overcome the singularities that arise using Keplerian Orbital Elements when dealing with circular and/or equatorial orbits.

Then, the NMPC problem has been formulated and the explicit input control law has been obtained taking advantage of PMP and so solving the dual optimization problem.

At the end, the autonomous space mission has been simulated in MATLAB/Simulink environment and the tuning of the NMPC parameters has been performed by trial and error procedure. The results obtained have fulfilled the design requirements.

Future Works

Further improvements and/or developments can be done starting from this work of thesis. For example a more realistic mathematical model can be used by adding disturbances, like non-spherical gravitational acceleration, aerodynamic drag and secondary body perturbations effects. Boundary conditions for the mass state variable can be found in order to add it on the optimization problem based on PMP. An high-thrust strategy, with a possible use of shaping function, can be adopted, in order to highlight the main differences with strategy used in the work

of thesis (low-thrust). At the end, a feasibility study about non-coplanar transfer space mission can be done, considering both low and high thrust strategies.

Bibliography

[1] *Satellite.* URL: https://en.wikipedia.org/wiki/Satellite (cit. on p. 1).

[2] *Low Earth Orbit.* URL: https://en.wikipedia.org/wiki/Low_Earth_orbit (cit. on pp. 1, 3).

[3] *Advantages and disadvantages of LEO.* URL: https://www.rfwireless-world.com/Terminology/Advantages-and-Disadvantages-of-LEO-orbit.html (cit. on p. 2).

[4] *Geostationary Orbit.* URL: https://en.wikipedia.org/wiki/Geostationary_orbit (cit. on p. 3).

[5] *Advantages and disadvantages of GEO.* URL: https://www.rfwireless-world.com/Terminology/Advantages-and-Disadvantages-of-GEO-Geosynchronous-orbit.html (cit. on p. 4).

[6] M. Pagone, M. Boggio, C. Novara, L. Massotti, and S. Vidano. «A Sparse Nonlinear Model Predictive Control for Autonomous Space Missions». In: *71st International Astronautical Congress (IAC) – The CyberSpace Edition* (Oct. 2020) (cit. on p. 6).

[7] L.S. Pontryagin, V.G. Boltyanskii, R.V. Gamkrelidze, and E.F. Mishchenko. *The Mathematical Theory of Optimal Processes.* Ed. by L.W. Neustadt. New York: Interscience Publisher, John Wiley and Sons, 1962 (cit. on pp. 6, 38).

[8] C. Novara. «Nonlinear Control and Aerospace Applications : lecture notes». In: Politecnico di Torino, 2017 (cit. on pp. 8, 10, 11, 23, 31, 35).

[9] *Modified Equinoctial Orbital Elements.* URL: https://spsweb.fltops.jpl.nasa.gov/portaldataops/mpg/MPG_Docs/Source%20Docs/EquinoctalElements-modified.pdf (cit. on p. 25).

[10] *True longitude.* URL: https://en.wikipedia.org/wiki/True_longitude (cit. on p. 25).

[11] Giovani Cavalcanti Nunes. *Design and analysis of multivariable predictive control applied to an oil-water-gas separator: a polynomial approach.* 2001. URL: https://citeseerx.ist.psu.edu/viewdoc/download?doi=10.1.1.6.6300&rep=rep1&type=pdf (cit. on p. 29).

[12] E.F. Camacho and C. Bordons. *Model Predictive control.* Ed. by Springer-Verlag London. Second. 2007 (cit. on p. 30).

[13] M. Boggio. «Spacecraft Autonomous Guidance and Control». In: *Politecnico di Torino* (July 2019). URL: `https://webthesis.biblio.polito.it/11647/1/tesi.pdf` (cit. on pp. 33, 35, 37, 45).

[14] M. Pagone, M. Boggio, C. Novara, and S. Vidano. «A Pontryagin-based NMPC approach for autonomous rendez-vous proximity operations». In: *2021 IEEE Aerospace Conference* (Mar. 2021) (cit. on p. 37).

[15] A.E. Bryson and Y. Ho. *Applied optimal control: optimization, estimation and control.* Taylor and Francis Inc., 1975 (cit. on p. 39).

[16] M.C.V. Salgado, M.C.N. Belderrain, and T.C. Devezas. «Space Propulsion: a Survey Study About Current and Future Technologies». In: *Journal of Aerospace Technology and Management* (2018) (cit. on p. 48).

[17] *Electric propulsion.* URL: `https://descanso.jpl.nasa.gov/SciTechBook/series1/Goebel_01_Chap1_Intro.pdf` (cit. on p. 50).